AD-A093 939 BRISTOL UNIV (ENGLAND) H H WILLS PHYSICS LAB F/G 11/1
STATES OF STRESS AND STRAIN IN ADHESIVE JOINTS INCLUDING PHOTOE--ETC(U)
NOV 80 K H ASHBEE, N R FARRAR, N K KITSON AFOSR-77-3448
UNCLASSIFIED AFOSR-TR-80-1358 NL

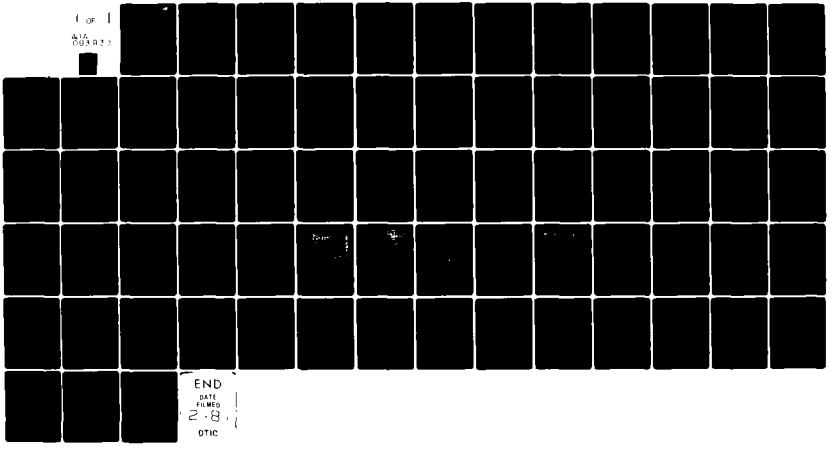

END
DATE FILMED
2-81
DTIC

Grant Number: AFOSR-77-3448

STATES OF STRESS AND STRAIN IN ADHESIVE JOINTS INCLUDING PHOTOELASTIC IMAGING OF DEFECTS IN ADHERENDS

N R Farrar
N K Kitson
S A Low
A Mears
J P Sargent
T W Turner
K H G Ashbee

H H Wills Physics Laboratory, Bristol University, England

November 30th 1980

Final Scientific Report, September 30th 1977 - September 30 1980

Approved for public release; distribution unlimited

prepared for

UNITED STATES AIR FORCE

AIR FORCE OFFICE OF SCIENTIFIC RESEARCH

Building 410, Bolling Air force Base, D.C. 20332

and

EUROPEAN OFFICE OF AEROSPACE

RESEARCH AND DEVELOPMENT

223/231 Old Marylebone Road, London NW1 5TH

SECURITY CLASSIFICATION OF THIS PAGE (When Data Entered) UNCLASSIFIED

REPORT DOCUMENTATION PAGE	READ INSTRUCTIONS BEFORE COMPLETING FORM
1. REPORT NUMBER (18) AFOSR (19) TR-80-1358	2. GOVT ACCESSION NO. AD-A093 939
	3. RECIPIENT'S CATALOG NUMBER rept.
4. TITLE (and Subtitle) (6) STATES OF STRESS AND STRAIN IN ADHESIVE JOINTS INCLUDING PHOTOELASTIC IMAGING OF DEFECTS IN ADHERENDS	5. TYPE OF REPORT & PERIOD COVERED (9) FINAL 30 Sept 77-30 Sept 80
	6. PERFORMING ORG. REPORT NUMBER
7. AUTHOR(s) (10) K. H. G. ASHBEE, N. R. FARRAR, N. K. KITSON, S. A. LOW, A. MEARS, J. P. SARGENT, T. W. TURNER	8. CONTRACT OR GRANT NUMBER(s) (15) AFOSR-77-3448 DAH-EF.0-76-G-068
9. PERFORMING ORGANIZATION NAME AND ADDRESS H H WILLS PHYSICS LABORATORY BRISTOL UNIVERSITY ENGLAND	10. PROGRAM ELEMENT, PROJECT, TASK AREA & WORK UNIT NUMBERS 61102F (17) (16) 2307/B2
11. CONTROLLING OFFICE NAME AND ADDRESS AIR FORCE OFFICE OF SCIENTIFIC RESEARCH NA BOLLING AFB DC 20332	12. REPORT DATE November 30 1980
	13. NUMBER OF PAGES 62
14. MONITORING AGENCY NAME & ADDRESS (if different from Controlling Office) (11) 30 Nov 80 (12) 71	15. SECURITY CLASS. (of this report) UNCLASSIFIED
	15a. DECLASSIFICATION DOWNGRADING SCHEDULE

16. DISTRIBUTION STATEMENT (of this Report)

Approved for public release; distribution unlimited

17. DISTRIBUTION STATEMENT (of the abstract entered in Block 20, if different from Report)

18. SUPPLEMENTARY NOTES

19. KEY WORDS (Continue on reverse side if necessary and identify by block number)

EPOXY
ADHESIVE JOINTS
FRACTURE MECHANICS
PHOTOELASTIC IMAGING
DEFECTS

20. ABSTRACT (Continue on reverse side if necessary and identify by block number)

Water migration across the thin epoxy layer in model adhesive joints causes strongly inhomogeneous swelling. The swelling is the principal cause of stress systems which are being examined by analysis of the patterns of Newton's rings formed between a glass cover slip and an optical flat. Enhancement of water migration by normal stresses of the order of a kilobar is reported. The development of a self-stressed fracture mechanics test piece, designed to investigate water uptake by adhesives, is reported. Photoelastic imaging of ultrasonic waves can be utilized to investigate

DD FORM 1 JAN 73 1473 EDITION OF 1 NOV 65 IS OBSOLETE A UNCLASSIFIED 5/N 0102-014-6601

SECURITY CLASSIFICATION OF THIS PAGE (When Data Entered)

defects in opaque solids. Instead of using a piezoelectric detector, the reflected sound from a defect is actually observed in a visualizing block of quartz, after propagating from the specimen to the block across an acoustic coupling. Experiments and a computer model are described.

SUMMARY

Water migration across the thin epoxy layer in model adhesive joints causes strongly inhomogeneous swelling. The swelling is the principal cause of stress systems which are being examined by analysis of the patterns of Newton's rings formed between a glass cover slip and an optical flat. Enhancement of water migration by normal stresses of the order of a kilobar is reported.

The development of a self-stressed fracture mechanics test piece, designed to investigate water uptake by adhesives, is reported.

Photoelastic imaging of ultrasonic waves can be utilized to investigate defects in opaque solids. Instead of using a piezoelectric detector, the reflected sound from a defect is actually observed in a visualizing block of quartz, after propagating from the specimen to the block across an acoustic coupling. Experiments and a computer model are described.

TABLE OF CONTENTS

LIST OF FIGURES

1. INTRODUCTION

Water migration rates in resin layers, sufficiently thin to be representative of the resin between adherends in an adhesive joint, were studied with support from the US Army European Research Office under grant number DA-ERO-76-G-068. Both polyester and epoxy resin samples containing entrapped air bubbles were cast between glass microscope slides and immersed in water. The times at which droplets of water appeared inside the air bubbles, distributed at varying distances from the edge of the resin layer, were noted allowing the rates of water uptake to be determined. The results, reported in a seminar presented by K H G Ashbee at AMMRC, Watertown, Mass on 23 July 1976, give diffusion coefficients of $\sim 10^{-4} cm^2 s^{-1}$ for polyesters and $\sim 10^{-7} cm^2 s^{-1}$ for epoxies; both faster than the published diffusion coefficients in the bulk resin, by about an order of magnitude.

During the first year of tenure of AFOSR-77-3448, careful consideration was given to the mechanisms which might explain the apparent enhancement of water migration. Four possibilities are:

(i) increased water flow through channels or crazes associated with the infrastructure of the interfacial region,

(ii) stress enhanced migration resulting from the stresses induced by shrinkage that accompanies curing,

(iii) stress enhanced migration caused by differential contraction on cooling from the curing temperature,

(iv) stress enhanced migration effected by the stress system produced by resin swelling on water uptake.

Evidence in support of the first of these hypotheses has not been found, and recent studies involving microscopic examination certainly have revealed some characteristic of channels had they been present. Similarly, the second possibility is a most unlikely mechanism, for curing takes place above Tg where dimensional changes will almost certainly be taken up by viscoelastic flow. Some stress system will remain from the third mechanism although partial relief of the forces is anticipated by self adjustment of the glue line thickness, but a more important source of stress is that of the fourth mechanism above. This swelling of the resin due to water uptake has been shown to be strongly inhomogeneous, and is believed to be the principal cause of stress fields which account for the significant changes in the diffusion rates in fibre reinforced resins.

The Newton's rings experiment which has been developed to investigate water diffusion is the most precise way of investigating water migration in stressed epoxies, and a theoretical model has been devised to probe the physical mechanisms. The classical diffusion equation has been modified by introducing a stress induced flux term, and the influence of internal stresses on the activation energy is considered. The epoxy resin, at operating temperatures substantially below the glass transition, is treated as purely elastic.

The urgent need for a fracture mechanics test, which might be used to observe the effects of water uptake on K_{IC} in adhesive joints, was made evident at the workshop on structural adhesives, organised by AFOSR and held at Vought Corporation, Grand Prairie, Texas in December 1977. Some useful ideas have been developed and after discarding the original test-piece, the validity of the latest self-stressed fracture mechanics test-piece has been shown. There are still some interesting features of the stress system to be analysed, as there are differences between the theory and practical considerations. For example, the theory requires a set of boundary conditions which cannot be achieved in practice, but can be approximated to by the application of a quite different stress system. When the test is carried out the stress system should revert to that which is used in the theoretical approach, but a doubt has arisen that this transition does in fact occur. This work is however at an advanced stage and is continuing unsupported by outside funds.

Much of the work associated with water uptake causing resin swelling, and with fracture mechanics tests results in defects of one kind or another, and a need arose to generate direct evidence for the location and size of such defects. In view of the progress made in previous photoelastic imaging experiments relating to a project on the physical mechanisms responsible for the weathering of epoxy resins and GFR epoxy resins (US Army grant DA-ERO-76-G-068) a natural development was to use photoelastic imaging of interference caused by defects. The interference patterns are generated in ultrasonic wave trains and carry information which allow cracks, voids, and holes to be located. By acoustically coupling a specimen to a transparent visualizing block, information about defects in opaque specimens can be found. Attention has been focused on a computer model which investigates the waves originating from a transducer probe and those waves which emanate from a defect or fault.

A series of tests has proceeded in parallel with the computer model, but as attempts have been made to detect smaller and smaller defects, increased frequency requirements have led to difficulties. At frequencies above 10 MHz there is a significant increase in the attentuation of the ultrasound, and resin based specimens including those for adhesive joints and film composites dissipate the stress waves rapidly. With some energy

always lost at the interfaces of the two phases of composite specimens, it is anticipated that the development of ultrasonic methods in non-destructive evaluation will be limited.

2. NEWTON'S RINGS EXPERIMENT

2.1 EXPERIMENTATION

The method used to investigate swelling of the adhesive is to measure the displacement normal to an adhesive layer. Accurate measurements can be achieved by observing Newton's rings, perhaps more correctly described as Fizeau interference fringes, created by having one of the adherends sufficiently thin to allow flexing and in contact with a reference flat. The specimen consists of a thoroughly cleaned glass cover slip (the thin flexible adherend) bonded to a thoroughly cleaned rigid block of glass or metal. With monochromatic light, a complex pattern of interference fringes is formed from the cover slip and optical flat reflections, which precisely define the topology of the cover slip and therefore of the underlying resin. Should the shape of the cover slip change, as happens when the resin swells during water uptake, the pattern of interference fringes changes.

The experimental arrangement is shown in Figure 1. Light from a mercury vapour discharge lamp is directed through an interference filter, a collimating lens, a half-silvered mirror, an optical flat, and the cover slip. Interference between incident and reflected beams occurs within the variable thickness gap located between the cover slip and optical flat. The interference pattern is photographed using the light reflected into a 35 mm camera by the half-silvered mirror.

The pattern of interference fringes is determined by the geometry of the gap between cover slip and optical flat and, to ensure that changes in the pattern arise only from distortion of the cover slip caused by resin swelling, it is essential that each run be carried out without disturbing the specimen/optical flat assembly. All of the components are set up on an optical bench. Figures 2 and 3 show general views of the ambient temperature and high temperature ($<100^{o}C$) apparatus respectively.

Enhancement of fringe contrast as a consequence of multiple beam interference can be obtained by fully silvering the upper surface of the cover slip and partially silvering of the lower surface of the optical flat. A range of reflective coatings has now been evaluated from which it is evident that a chromium layer is most effective, having sufficient

water resistance to withstand a full length boiling water test. The main disavantages of a chromium layer are that it obscures direct observations of the adhesive and is difficult to remove should it need renewing. An alternative and very successful method for securing multiple beam interference and hence for improving fringe definition has been realised by using a wedge shaped optical flat. With a wedge angle of 4^{o} the image of the Newton's rings does not coincide with reflections from other glass or water surfaces. The wedge is made from flint glass with refractive index 1.65 and has been incorporated into a mark II version of the hot water apparatus designed to permit undisturbed tests at any fixed temperature between ambient and $100^{o}C$. This is shown in Figure 4.

Whilst direct observation of this interference pattern can be used to measure increments of swelling, the changing geometry is obtained directly by superimposing successive images of the pattern photographed during water uptake, on the pattern photographed before swelling. Superimposition produces Moiré fringes, the development of which faithfully follows any changes in the shape of the cover slip.

Moiré fringes are generated when patterns with nearly identical periodic structures are made to overlap. In this instance, photographic images of the interference pattern form the periodic structures and differences in the pattern, seen on comparing the image photographed before swelling with images taken during swelling, gives rise to the Moiré effect. In Figure 2, the Moiré fringes are the circumferential lines running around the rim of the specimen and are superimposed upon the interference pattern. (It should be noted that the broad dark almost parallel bands running across the specimen are due to tilting with respect to the optical flat). As water diffuses into the specimen, new interference fringes are generated at the edge and migrate towards the centre, each fringe representing the locus of points of constant displacement normal to the joint. Similarly in the Moiré pattern, a new Moiré fringe is generated and migrates in from the edge of the specimen whenever a new interference fringe is generated. Thus successive Moiré fringes map out the loci of positions which differ in displacement normal to the joint by half a wavelength. Hence the number of Moiré fringes N to have passed a given point is simply related to the normal displacement of the joint w by:

$$w = \frac{N\lambda}{2\mu}$$

where λ = wavelength of light
μ = refractive index of the immersion liquid

Specimens usually took the form of a circular glass cover slip bonded to a rigid block of metal such as stainless steel or anodised titanium. However, some specimens were manufactured using cover slips which were both square in outline and of different thickness. This was done in order to investigate the effects of varying the mechanical constraint attributable to cover slip geometry.

2.2 WATER ABSORPTION MODEL

Consider the adhesive specimen of the previous Section in cylindrical polar coordinates and assume axial symmetry.

Let $\underline{J}(r,t)$ denote the flux of water molecules passing perpendicular through a reference surface of unit area during unit time. $\underline{J}$ may be expressed in terms of the local mass velocity $\underline{u}$ of the water molecule by

$$\underline{J}(r,t) = c(r,t).\underline{u}(r,t)$$

where $c(r,t)$ is the local concentration of water molecules, at time t. No mechanism of migration need be specified at this point.

The aim is to investigate the influence of the internal stress field which causes changes in both $c(r,t)$ and $\underline{u}(r,t)$.

Fick's second law,

$$\frac{\partial c}{\partial t} = \frac{\partial}{\partial x}\left\{D(c)\frac{\partial c}{\partial x}\right\}$$

gives the concentration of a diffusing species in one dimension. D, the diffusion coefficient can often be taken as constant, but in the diffusion of polymers it is a function of concentration. When extensive swelling of a polymer is caused by the penetrant, non-Fickian diffusion has been observed, Kwei and Zupko (1969), Alfrey et al (1966).

Non-Fickian behaviour may be directly related to the influence of the changing polymer structure on the solubility and differential mobility, or may result from the internal stresses exerted by one part of the medium on another as diffusion proceeds. Polymers usually have a wide spectrum of relaxation times associated with structural changes and a sorption process will be influenced by those segmental motions which occur at about the same rate or slower than the motivating diffusion process. Alfrey, Gurnee and Lloyd (1966) proposed a useful classification according to the relative rates of diffusion and polymer relaxation. Three classes are distinguished:

(I) Fickian diffusion in which the rate of diffusion is much less than that of relaxation.
(II) Diffusion in which the rate is very rapid compared with the relaxation process.
(III) Non-Fickian or anomalous diffusion which occurs when the diffusion and relaxation rates are comparable.

The following assumptions are made in the development:

Epoxy resins are assumed to be isotropic and homogeneous.
The specimen is treated as having axial symmetry at all times.
Activated diffusion forms the main contribution to the migration of water molecules within the epoxy.
No increased migration of water takes place along the glass/epoxy interface due to any deterioration of interfacial bonding.
Water uptake produces stresses which are not sufficiently large to form microcracks and channels.
Effects of gravity are negligible.
The epoxy resin behaves as perfectly elastic for the internal stresses and strains caused by water uptake.
The elastic constants are unchanged by the water concentrations encountered in the epoxy resin.
The compressive forces at the rim of the specimen resulting from inhomogeneous swelling have negligible effect on the saturation concentration at the outer surface, and that this equilibrium saturation concentration is reached instantaneously.

In the following, two different models for the effect of stress on water uptake will be considered. It will become apparent that a very important quantity in such models is the concentration gradient. A large concentration gradient implies a large flux of water molecules by Fick's First Law, which gives

$$J = -D \frac{\partial c}{\partial x} \qquad 2.1$$

In addition, however, a large concentration gradient implies a large stress-field and thus possibly a significant stress-induced flux. In subsequent paragraphs consideration will be given to the effect of the stress-field on the mobility and thus on the diffusion coefficient D. A stress-induced flux term in Fick's First Law will also be introduced.

It will be convenient to use the word "system" to refer to the epoxy resin contained between the cover-slip and the microscope slide plus any water molecules that have diffused into it. The word "specimen" will refer to the complete model adhesive joint, i.e. the epoxy resin plus the glass

cover-slip and microscope slide.

Now consider a water molecule within the epoxy resin. On average it will make ϕ jumps per unit time with a distance δ per jump. Then the diffusion coefficient will be given by an expression similar to

$$D = \frac{1}{6} \phi \delta^2 \qquad 2.2$$

Now δ the jump distance will clearly depend on the state of the system; that is, one would expect the jump distance in a region under compression to be less than that in an unstressed region. It will be assumed for the moment, however, that the jump distance remains constant and consideration will be given to the effect of stress on the number of jumps per unit time, ϕ.

Let v_f denote that volume within the system which is effectively free to a diffusing species to occupy without the necessity to perform work on the surrounding polymer molecules. For an unstressed specimen one would expect this volume to vary throughout the system as a result of the fluctuations in thermal energy of the constituent polymer molecules. Therefore, consider the mean value of v_f, to be denoted by $\bar{v}_f$, which will be referred to as the "free volume". In a region of the polymer which is under compression $\bar{v}_f$ would be expected to decrease from its unstressed value and in a region under tension one would anticipate $\bar{v}_f$ to increase. Thus for a system in which there exists a stress-field

$$\bar{v}_f = \bar{v}_f \ (r,z,t)$$

Now returning to ϕ, the number of jumps per unit time, one can see that

$$\phi = f(E_{th} \bar{v}_f)$$

where E_{th} denotes the thermal energy of the water molecule being considered and f is a function to be determined. If the effective volume of the water molecule, v_w, in the system is greater than the free volume $\bar{v}_f$ then work will have to be done on the polymer molecules surrounding the free volume to permit the water molecule to jump. The energy to perform this work must come from the thermal fluctuations. The probability that the water molecule has thermal energy E'_{th} is proportional to the Boltzmann factor $e^{-E'_{th}/KT}$. Now for a jump to occur one must have $E'_{th} > E^*$ where E^* denotes the energy equivalent of the minimum performed work in jumping plus, possibly, some constant energy term. Hence the probability of jump Pr is proportional to

$$\{\int_{E^*}^{\infty} e^{-E'_{th}/kT}\, dE'_{th}\}/\{\int_{o}^{\infty} e^{-E'_{th}/kT}\, dE'_{th}\}$$

giving $Pr \propto e^{-E^*/kT}$ where E^* is called the activation energy of the process. Hence $\phi \propto e^{-E^*/kT}$ and, subsequently, from 2.2 one obtains $D \propto e^{E^*/kT}$. If one assumes that variations in the jump distance δ have a negligible effect on D compared to variations in ϕ then a possible expression for the diffusion coefficient would be

$$D = D_o e^{-E^*/kT} \qquad 2.3$$

An alternative way of analysing the diffusional jump is to think of the fluctuations in local free volume v_f due to the thermal fluctuations of the energy of the polymer chains. Then a water molecule will only jump if a sufficiently large free volume v_f ($= v_w$) exists adjacent to its present site. Thinking in terms of the free volume as consisting of discrete, independent entities one may use the term hole instead of free volume. If an energy E_h is associated with a hole of size v_f then the probability that a hole of size v_f can be found is, according to the Boltzmann distribution, proportional to $\exp(-E_h/kT)$. The average size of a hole in the material is then given by the following expression

$$\bar{v}_f = \{\int_o^{\infty} v_f e^{-E_h/kT}\, dv_f\}/\{\int_o^{\infty} e^{-E_h/kT}\, dv_f\}$$

Also the fraction of holes having volume v_w or greater is

$$\{\int_{v_w}^{\infty} e^{E_h/kT} dv_f\}/\{\int_o^{\infty} e^{-E_h/kT} dv_f\} \qquad 2.4$$

In writing equation 2.4 one is assuming that the holes are discrete and independent but in reality this is not so. Even if an individual hole may not be large enough to accommodate a diffusing molecule, the co-operative motion of several neighbouring molecules may allow two or more holes to merge into one hole large enough for a diffusional jump to occur. Thus the fluctuations in free volume will be brought about by complex configurational changes of the polymer molecules and one would anticipate that an expression involving the various degrees of freedom available to the polymer molecules would be obtained instead of 2.3. This is in fact true and many expressions have been proposed (see, for example, Crank and Park [1968] and Barrer [1941]).

Returning to equation 2.3 it is assumed that E^* can be written in the form

$$E^* = E_w + E_c \qquad 2.5$$

where E_w is the energy equivalent of the work done by a water molecule in a diffusional jump and E_c is some constant energy term which includes that part of the energy required by the water molecule to change locations even

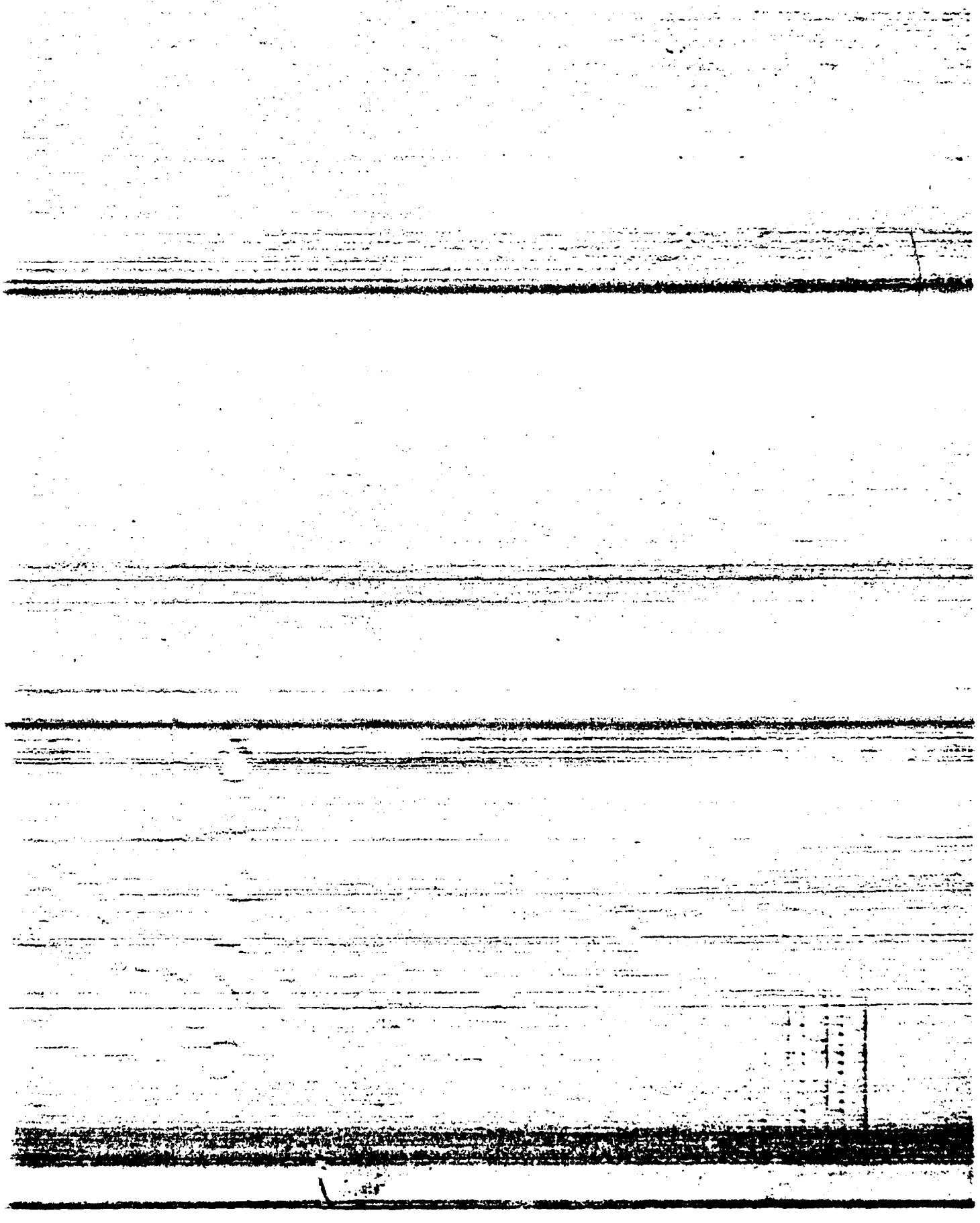

if the free volume is equal to or greater than the volume v_w. Consider a spherical cavity of radius r_f at the centre of a sphere of large radius R.

Let r_f and r_w be given by

$$\bar{v}_f = \frac{4}{3}\pi r_f^3, \quad v_w = \frac{4}{3}\pi r_w^3$$

It will be assumed that a suitable approximation for E_w is

$$E_w = Pr_f \to r_w \ (v_w - \bar{v}_f) \qquad 2.6$$

where $Pr_f \to r_w$ is the pressure required to change the radius of the central cavity from r_f to r_w. Using elasticity theory one obtains

$$Pr_f \to r_w = \frac{2\Gamma}{(1+\nu)}\{\eta(r,t) - 1\} \qquad 2.7$$

where $\eta = r_w/r_f > 1$.

Now clearly as water molecules migrate through the system, and a continuously changing stress-field is set up, then the free volume $\bar{v}_f$ will change from its initial unstressed value $\bar{v}_{fi}$. In order to estimate this change in free volume $\bar{v}_f$ consider a thin spherical shell of thickness s where $\bar{v}_f$ is represented by the spherical interior of this shell.

Assuming that r_f is small then $1/3\sigma_{ii}(r,z,t)$ is approximately the average value of the normal component of stress over the surface of the shell with centre at a point (r,z) at time t. Thus it is reasonable to take the pressure P_s at the surface to be given by

$$P_s(r,z,t) = -1/3\sigma_{ii}(r,z,t)$$

where σ_{ii} is assumed known, and determined by elasticity theory. To remove the z-dependence of this pressure consider an average over the z-coordinate:

$$P_s(r,t) = -1/3h\int_0^h \sigma_{ii}(r,z,t)dz$$

where $\sigma_{ii} = \sigma_{rr} + \sigma_{\theta\theta} + \sigma_{zz}$ and h is the thickness of the system. Assuming the thickness of the shell to be small relative to r_f elasticity theory yields

$$u = -\frac{P_s\ (1 - \nu)\ r_f^2}{2Es}$$

Thus the new free volume $\bar{v}_{fn}$ is obtained from the old free volume $\bar{v}_{fo}$ by

$$\bar{v}_{fn} = \frac{4\pi}{3}\left(\left(\frac{3v_{fo}}{4\pi}\right)^{1/3} + u\right)^3$$

$$\simeq \bar{v}_{fo}\left(1 - \frac{\lambda(\bar{v}_{fo})^{1/3}p_s}{S}\right) \qquad 2.8$$

where $\lambda = 3\left(\frac{3}{4\pi}\right)^{1/3}\left(\frac{1-\nu}{2E}\right)$

Thus combining 2.3, 2.5, 2.7 and 2.8 one obtains

$$D = D'_o \exp\left[-\frac{\alpha(\eta-1)}{kT}\{v_w - \bar{v}_{fo} + \lambda\xi P_s\}\right] \qquad 2.9$$

when $v_w > v_{fn}$, where

$D'_o = D_o \exp[-Ec/kT]$, $\eta = \frac{r_{fn}}{r_w}$, $\alpha = \frac{2E}{(1+\nu)}$, $\xi = \frac{(v_{fo})^{4/3}}{S}$, $v_{fo} = 4/3\pi r_{fo}^3$,

and $P_s = -1/3h\int_o^h \sigma_{ii}\, dz$

If $v_w < \bar{v}_{fn}$ then $D = D_o \exp[-Ec/kT]$ and no swelling should be observed.

Having investigated the effect of stress on the mobility and hence the diffusion coefficient, the possibility of a stress-induced flux will now be considered. It should be noted that these two models proposed, are different ways of modelling the same effect, i.e. the effect of the internal stress-field, resulting from water uptake, on the subsequent water migration. An attempt to combine the two models would be incorrect.

Firstly irreversible thermodynamics will be used to derive an equation for the migrtion of water molecules which incorporates a term which can be interpreted as a stress-induced flux. The equation to be derived is similar to that proposed by Frisch et al (1969) to model Case II swelling (see Page 3).

Consider an element of volume V of the system. Let there by n molecules of water in this volume, with velocity $\underline{v}_i$ and denote their centre of mass velocity by $\underline{v}_w$.

Then $$\underline{v}_w = \sum_{i=1}^{n} \underline{v}_i$$

Let the centre of mass velocity of the polymer molecules be $\underline{v}_p$. Then the centre of mass velocity $\underline{v}_c$ of all molecules within the volume V will be given by

$$\rho \underline{v}_c = \rho_w \underline{v}_w + \rho_p \underline{v}_p$$

where ρ_w and ρ_p are the densities of the water molecules and the polymer molecules respectively and $\rho = \rho_w + \rho_p$. The flux of water molecules defined with respect to the centre of mass frame is given by

$$\underline{J}_w = c_w(\underline{v}_w - \underline{v}_c) \quad (= -\underline{J}_p)$$

where c_w (the concentration of water molecules) $= \rho_w/\rho$, and the conservation of mass gives

$$\rho \frac{D c_i}{Dt} + \nabla \cdot (\rho \underline{J})_i = 0 \quad i = w,p \qquad 2.10$$

where $\frac{D}{Dt} \equiv \frac{\delta}{\delta t} + \underline{v}_c \cdot \nabla$

It will be assumed that the equation of motion may be written in the form:-

$$\rho \frac{D}{Dt}(\underline{V}_c)i = \sum_{k=w,p} \rho_k (\underline{F}_k)_i + \frac{\partial p_{ij}}{\partial x_j} \quad (i,j = 1,2,3)$$

by analogy with fluid dynamics, where p_{ij} is the stress tensor, and the forces $\underline{F}_k$ will be assumed zero. The energy equation for u, the energy per unit mass, with the exclusion of the centre of mass kinetic energy is

$$\rho \frac{D}{Dt}\left(\frac{1}{2}(\underline{V}_c)^2 + u\right) = \frac{\partial}{\partial x_j}(P_{ij}(\underline{V}_c)_i)$$

Elimination of $(\underline{v}_c)^2$ using the equation of motion gives

$$\rho \frac{Du}{Dt} = P_{ij} \frac{\partial (\underline{V}_c)_i}{\partial x_j} \qquad (i,j = 1,2,3) \qquad 2.11$$

The Second Law of Thermodynamics gives

$$T \frac{DS}{Dt} = \frac{DU}{Dt} + p\frac{DV}{Dt} - \sum_{k=w,p} \mu_k \frac{DM_k}{Dt} \qquad 2.12$$

where μ_w and M_w are the chemical potential and total mass of the water molecules, respectively; μ_p and M_p are the chemical potential and total mass of the polymer molecules, respectively; S is the total entropy and U the total energy. The quantity, p, in 2.12, denoting the pressure can be defined to be equal to $-1/3 p_{ii}$, and for convenience let

$$P_{ij} = -p\delta_{ij} + d_{ij} \qquad 2.13$$

where $d_{ii} = 0$.

Changing to intensive quantities 2.12 becomes

$$T \frac{Ds}{Dt} = \frac{Du}{Dt} + p\frac{Dv}{Dt} - \sum_{k=w,p} \mu_k \frac{Dc_k}{Dt} \qquad 2.14$$

Now substituting 2.13 into 2.11 gives

$$\rho\frac{Du}{Dt} = -p\ \nabla.\underline{V}_c + d_{ij}\frac{\partial(\underline{v}_c)_i}{\partial xj} \qquad (i,j = 1,2,3)$$

But $$\frac{D\hat{\rho}}{Dt} = -V^{-2}\frac{Dv}{Dt} = -\rho\nabla.\underline{V}_c ,$$

thus $$\frac{Du}{Dt} = -p\frac{Dv}{Dt} + \frac{d_{ij}}{\rho}\frac{\partial(\underline{V}_c)_i}{\partial x_j} \qquad 2.15$$

Introducing 2.10 and 2.15 into 2.14 gives

$$\rho T\frac{Ds}{Dt} = d_{ij}\frac{\partial(\underline{V}_c)_i}{\partial x_j} + \sum_{k=w,p} \mu_k\nabla.(\rho\ \underline{J}_k) \qquad (i,j = 1,2,3) \qquad 2.16$$

Now diffusion is an irreversible phenomenon which can be expressed to a first approximation by linear phenomenological relations of the general type

$$J_i = \sum_{k=1}^{m} L_{ik}\ X_k \qquad (i = 1,2, \ldots, m)$$

for an m-component system where J_i denotes the flux of the i^{th} component, X_i denotes a "force" (e.g. concentration gradient, potential gradient), and the coefficients L_{ik} $(i,k = 1,2,\ldots,m)$ are called the phenomenological coefficients (see, for example, Bearman and Kirkwood (1958), Bearman (1958), De Groot (1951).

Now 2.16 can be rewritten in the form

$$\rho\frac{Ds}{Dt} = \sum_{k=w,p} \nabla.\left(\frac{\mu_k\rho\underline{J}_k}{T}\right) + \frac{dij}{T}\frac{\partial(\underline{V}_c)_i}{\partial xy} + \sum_{k=w,p}\frac{\underline{J}_k.\underline{X}_k}{T} \qquad 2.17$$

where $$\underline{X}_k = -\rho\nabla\mu_k \qquad 2.18$$

for isothermal diffusion.

Note the term $\frac{d_{ij}}{T}\frac{\partial(\underline{v}_{ci})}{\partial x_j}$ will have no influence on the form of the phenomenological relations

$$\underline{J}_w = L_{ww}\underline{X}_w + L_{wp}\underline{X}_p$$

$$\underline{J}_p = L_{pw}\underline{X}_w + L_{pp}\underline{X}_p$$

since the force in this term (i.e. $\partial(\underline{V}_c)_i/\partial x_j$) has a tensorial character and cannot give rise to vectorial fluxes $\underline{J}_i$ (Curie's theorem).

Now it can be shown (See De Groot [1951]) that

$$L_{ww} + L_{wp} = 0,\ L_{pw} + L_{pp} = 0,$$
$$L_{ww} + L_{pw} = 0,\ L_{wp} + L_{pp} = 0.$$

so that $$\underline{J}_w = -\underline{J}_p = L_{ww}(\underline{X}_w - \underline{X}_p) \qquad 2.19$$

Alternatively, since it was already known that $\underline{J}_p = -\underline{J}_w$ one could have used this in deriving 2.17 to give $\underline{X}_w = -\rho\nabla(\mu_w - \mu_p)$, $\underline{X}_p = 0$ yielding the same results. Using 2.18 and 2.19 one obtains

$$\underline{J}_w = L_{ww}(-\rho\nabla\mu_w + \rho\nabla\mu_p)$$

$$= L_{ww}\rho\left[\left(\frac{\partial}{\partial p}(\mu_p - \mu_w)\right)_{T_1C_w}\nabla p + \left(\frac{\partial}{\partial C_w}(\mu_p - \mu_w)\right)_{T_1p}\nabla C_w\right] \qquad 2.20$$

Now $C_w d\mu_w + C_p d\mu_p = 0$ at constant T and p (- the Gibbs-Duhem relation) also $C_w + C_p = 1$. Now it is expected that $C_p >> C_w$, then

$$\left(\frac{\partial}{\partial c_w}(\mu_p - \mu_w)\right)_{T_1p} = -\left(1 + \frac{C_w}{C_p}\right)\left(\frac{\partial\mu_w}{\partial C_w}\right)_{T_1p}$$

$$\simeq -\left(\frac{\partial\mu_w}{\partial C_w}\right)_{T_1p}$$

also

$$\left(\frac{\partial\mu_p}{\partial p}\right)_{T_1C_w} << \left(\frac{\partial\mu_w}{\partial p}\right)_{T_1C_w}$$

Thus 2.20 becomes

$$\underline{J}_w = - L_{ww}\rho\left[\left(\frac{\partial \mu_w}{\partial p}\right)_{T_1 C_w} \nabla p + \left(\frac{\partial \mu_w}{\partial \mu_w}\right)_{T_1 p} \nabla C_w\right] \qquad 2.21$$

For non-ideal systems the chemical potential of the i^{th} component takes the form

$$\mu_i = \zeta_i(p,T) + RT \log f_i C_i \qquad 2.22$$

where $\zeta_i(p,T)$ is independent of composition, C_i denotes the concentration and f_i is the activity coefficient, due to G N Lewis (see for example, Prigogine [1967]). Substituting 2.22 into 2.21 one obtains

$$\underline{J}_w = - L_{ww}\rho \left[\left(\frac{\partial \zeta_w}{\partial p}\right)_T \nabla p + \frac{RT}{C_w} \nabla C_w\right]$$

Now Fick's First Law gives

$$\underline{J} = - D\nabla C$$

therefore let the diffusion coefficient be defined by

$$D = \frac{L_{ww}\rho RT}{C_w} \qquad 2.23$$

Then the flux of water molecules in the epoxy resin is given by

$$\underline{J}_w = -D\left(\nabla C_w + \frac{C_w}{RT}\left(\frac{\partial \zeta_w}{\partial p}\right)_T \nabla p\right) \qquad 2.24$$

where the term $\left(\frac{\partial \zeta}{\partial p}\right)_T$

will depend on the interaction forces between the water molecules and their neighbouring polymer molecules.

An alternative method of deriving an equation of the form 2.24 is to consider the probability of a water molecule jumping to the right or to the left (in one-dimension). For simplicity consider the one-dimensional case only, with position co-ordinate x. Suppose that the pressure in the epoxy resin $p(\equiv -1/3\sigma_{ii} \equiv p_s)$ decreases with increasing x - co-ordinate.

Then the probability of a water molecule jumping to the right, to a site at $x + \Delta x$, is given by an expression of the form

$$P_R = A_{exp}[-(a_1 + a_2 p(x + \Delta x))/kT]$$

using equation 2.9. Similarly the probability of a water molecule jumping to the left, to a site at $x - \Delta x$, is given by an expression of the form

$$P_L = A_{exp}[-(a_1 + a_2 p(x - \Delta x))/kT]$$

Thus the flux of water molecules due to the stress-field is given by

$$J_S = \mu(P_R - P_L)$$

$$\approx \frac{\mu A a_2}{kT} \{p(x - \Delta x) - p(x + \Delta x)\}$$

$$\approx -\frac{2\mu A a_2}{kT} \delta \frac{\partial p}{\partial x}$$

where Δx has been replaced by δ the mean jump distance and μ is some suitable proportionality factor.

Then the total flux, denoted by J_{TOT}, will be of the form

$$J_{TOT} = -D \left(\frac{\partial c}{\partial x} + \alpha c \frac{\partial p}{\partial x}\right)$$

similar to 2.24

2.3 RESULTS AND DISCUSSION

After the first two years of experimental work the models described in the previous Section were set up. These two models of the possible effect of an internal stress field on water migration in epoxy resins, can be represented by the following two equations:

$$\frac{\partial c}{\partial t} = \nabla.[D_o e^{-(a_1+a_2 p(r,t))/kT} \nabla C]$$

and

$$\frac{\partial c}{\partial t} = \nabla.[D(\nabla C + \alpha c \nabla p)]$$

where a_1 and a_2 are constants with α assumed constant. For both models it is important to have a knowledge of the pressure distribution $p(r,t)$ which may be obtained from elasticity theory. $\sigma_{ij}(r,t)$ is most conveniently arrived at by applying numerical methods such as finite difference or finite element methods. Thus one can proceed to values of $p(r,t) = -1/3\sigma_{ij}$ from which the values of the constants can be determined by matching computed concentrations, for a given time, to experimentally evaluated concentrations.

It is possible as a first approximation to use the normal stresses necessary to return the cover slip to its initial shape as the pressure, and here we could apply A E H Love's equation

$$p = R\nabla^4\omega$$

where $\omega = \delta(0)$ is the axial displacement, p the normal stress (pressure) and R the flexural rigidity. The cover slip is treated as a thin plate.

The exact nature of the effect of the cover slip on the stress field is however a major consideration, since replacement of the cover slip with another microscope slide would allow little deformation and surface stresses would become more significant.

The effect of the cover slip is not at all obvious as it is chosen for its flexibility but the tangential stresses exerted by the cover slip could form an important constraint on the system.

The first long term test was made at room temperature on a joint between a cover slip and cleaned, but not anodised. SIC aluminium. A general purpose epoxy resin containing entrapped air bubbles was used as adhesive. Hereafter, this adhesive will be referred to as adhesive A. Its full

identity, including hardener and accelerator, and the curing schedule used for it, are given in Table 1.

	RESIN SYSTEM	PROPORTIONS	GEL	CURE
		p.b.w.		
	Ciba Geigy			
	MY 750 (Diglycidyl ether of bisphenol A)	100		
A	HY 917 (Methyl tetrahydrophthalic anhydride)	85	2 hours at 100°C	4 hours at 150°C
	DY 062 (Triamyl ammonium phenate)	2		
	Bloomingdale			
B	FM 1000 (Nylon modified epoxy film)			1 hour at 170°C
	BR 1009/49 (Phenolic primer)		2 hours at 20°C	1 hour at 70°C
C	Ciba Geigy (modified epoxy film) Redux 312/5			1/2 hour at 120°C
D	Bloomingdale FM 73M (modified epoxy film)			1 hour at 120°C

Table 1. Adhesives and Curing Schedules.

Later tests were carried out on joints between a cover slip and substrates of both stainless steel and anodized titanium using the commerially available adhesive film system designated B in Table 1. All metal surfaces were cleaned and, where applicable, treated in accordance with commercially accepted practice. The metal based specimens were supplied by Westland Helicopters Ltd in the form of cleaned and pre-primed coupon specimens.

For tests employing the adhesive film systems designated C and D in Table 1 both adherends were glass. Preparation of the glass cover slip surfaces is less well standardised. The fundamental problem is removal of oxides of low surface energy. Chemical attack by common oxidising agents, e.g. nitric acid and hydrogen peroxide certainly remove a large fraction of these oxides. So too does exposure to the oxidising region of a naked flame. Sand blasting in order to roughen the surface and promote mechanical linkages, and application of coupling agents (silanes) have also been recommended. However, no combination of these treatments has yet produced a joint which, when it eventually debonds after prolonged exposure to water in the absence of externally applied stress, leaves fracture surfaces which do not include large areas of glass/adhesive interface.

In joints manufactured using liquid resin, a reproducible glue line thickness was achieved by simply allowing the cover slip to sink under its own weight. In joints made using solid adhesive film, the glue line thickness was controlled by clamping during the cure process.

Adjacent rings of the same colour (black or white) are loci of points for which the optical path length, in the space between cover slip and optical flat, differs by one wavelength. By the same token, a displacement in the pattern of Newton's rings by an amount equal to one ring width corresponds to a change in path length equal to one wavelength. By observing changes in the number of rings between fixed markers, such as entrapped air bubbles, displacements normal to the joint during water uptake can be measured to an accuracy of $\lambda/4$. If required, displacements which are at least as small as $\lambda/10$ can be measured by superimposition of images in order to create Moiré patterns.

The water concentration, and hence the swelling associated with water uptake, eventually saturates and thereafter a shoulder separating fully saturated from less than fully saturated resin, progressively moves inwards from the rim of the joint. This is shown schematically in Figure 5c. Figure 6 shows a sequence of images obtained, showing the development of swelling in a joint manufactured between anodized titanium and a glass cover slip using adhesive B and immersed in distilled water at approximately 80°C.

To maintain contact with the outer ring of uniformly swollen adhesive (Figure 5c), the adherends would each need to bend with curvature that is opposite to that inside the shoulder. Failure to adopt such "S" wise bending manifests itself as an interfacial crack, the occurrence of which is revealed as patches of bright contrast at the rim in Figure 6.

The positions of well-defined points in the patterns of Newton's rings may be measured as functions of time. Figure 7 shows a plot of the shoulder defining the extent of water saturation, and of the crack edge as functions of (time) for an aluminium joint manufactured with adhesive A and immersed in distilled water at 20 C.

Figure 8 shows a plot of the shoulder defining the extent of water ingress form the experiment reported in Figure 6.

Figure 9 shows a similar plot for a specimen manufactured using adhesive B but with a stainless steel substrate and for an immersion water temperature of 80°C. From the marked similarity in the results for anodized titanium and stainless steel it is concluded that the deformation is wholly within the adhesive and is independent of the adherend. Moiré patterns, generated by superimposition of interference patterns before and after swelling were used to obtain the data in Figure 10. These specimens were manufactured from adhesives C and D and measurements were made at a range of temperatures between ambient and 100°C.

If migration of water occurs at low water concentrations and is governed by Fick's law, plots of migration distance as a function of $(\text{time})^{1/2}$ should approximate to straight lines. The data points for specimens manufactured with adhesives A and B certainly do not approximate to straight lines. However those manufactured with adhesives C and D and which were studied using the more precise Moire measuring technique do suggest Fickian behaviour although the slopes of the graphs indicate activation energies that are much higher than normally expected for epoxy resins.

To draw a comparison of this apparent Fickian behaviour in the specimens with the theory, we can solve Fick's law in cylindrical polar coordinates, assuming axial symmetry:

$$\frac{\partial C}{\partial T} = \frac{\partial^2 C}{\partial R} + \frac{1}{R}\frac{\partial C}{\partial R}$$

where $T = Dt/a^2$, $R = r/a$, $C = c/c_{SAT}$ with D a constant diffusion coefficient.

By using a suitable substitution this equation is Bessel's of order zero, and a solution may be found. For small values of T, the infinite series is slow to converge and computation is impractical. As T increases however, it is possible to obtain series which converge quite rapidly. Such a series has been used to obtain the theoretical curve of Figure 11 for a Redux 312/5 epoxy at 62°C where the time is 334 hours. It was found experimentally that full saturation was represented by 14 fringes and the experimental results have been included in the Figure 11.

By using a suitable substitution this equation is Bessel's of order zero, and a solution may be found. For small values of T, the infinite series is slow to converge and computation is impractical. As T increases however, it is possible to obtain series which converge quite rapidly. Such a series has been used to obtain the theoretical curve of Figure 11 for a Redux 312/5 epoxy at 62°C where the time is 334 hours. It was found experimentally that full saturation was represented by 14 fringes and the experimental results have been included in the Figure 11.

3. SELF STRESSED FRACTURE MECHANICS TEST-PIECE

3.1 THE ELASTIC DISC IN PLANE STRAIN

The disc consists of a circle of aluminium which in plane polar co-ordinates is defined by the relations $0 \leq r \leq a$ and $0 \leq \theta \leq 2\pi$. It is stressed by removing a sector $0 \leq r \leq a$, $2\pi - \Omega \leq \theta \leq 2\pi$ and making an adhesive joint when the gap has been closed. Assuming that plane stress conditions are met, it is necessary to calculate the stress intensity factor, K_I, and the formation energy, W, for the crack $c \leq r \leq a$, $\theta = 0$. This has been done by superimposing the solutions of the resulting stress with those of K_I and W for a traction-free circumference and a symmetrical pressure loading.

The Airy function given by Mitchell (1899), Eshelby (1966)

$$\Psi(r,\theta) = a_o + b_o \ln r + c_o r^2 + d_o r^2 \ln r \qquad 3.1$$

may be used to find the stress and displacement fields:

$$\sigma_{rr}(r,\theta) = b_o r^{-2} + 2c_o + d_o(1 + 2 \ln r) \qquad 3.2$$

$$\sigma_{r\theta}(r,\theta) = 0 \qquad 3.3$$

$$\sigma_{\theta\theta}(r,\theta) = -b_o r^{-2} + 2c_o + d_o(3 + 2 \ln r) \qquad 3.4$$

$$u_r(r,\theta) = E^{-1}\{-b_o(1+\nu)r^{-1} + 2c_o(1-\nu)r + 2d_o(1-\nu)r \ln r - d_o(1+\nu)r\} \qquad 3.5$$

and

$$u_\theta(r,\theta) = 4E^{-1} d_o r\theta \qquad 3.6$$

Since the solution is required to satisfy the conditions

(i) $\sigma_{rr}(a,\theta) = \sigma_{r\theta}(a,\theta) = 0$, $0 \leq \theta \leq 2\pi$

(ii) $u_\theta(r, 2\pi) = r\Omega$ and

(iii) u_r and u_θ are bounded at $r = 0$, we see that $b_o = 0, d_o = E\Omega/8\pi$ and $c_o = -(E\Omega/8\pi) \ln(a\sqrt{e})$.

Therefore

$$\Psi(r,\theta) = \frac{F\Omega}{8} r^2 \ln(r/a\sqrt{e}) \qquad 3.7$$

and

$$\sigma_{\theta\theta}(r,0) = \frac{F\Omega}{4\pi} \{1 + \ln(r/a)\} \qquad 3.8$$

It follows that we may write $\sigma(r) = p_o f(r/a)$

where $p_o = F\Omega/4\pi$

and $f(\rho) = 1 + \ln\rho$

To find K_I and W the dimensionless quantities $\rho = r/a$ (already introduced) may be used

$$s_{\rho\rho}(\rho,\theta) = \frac{\sigma_{rr}(r,\theta)}{p_o}, \; s_{\rho\theta}(\rho,\theta) = \frac{\sigma_{r\theta}(r,\theta)}{p_o}, \; s_{\theta\theta}(\rho,\theta) = \frac{\sigma_{\theta\theta}(r,\theta)}{p_o} \qquad 3.9$$

$$u(\rho,\theta) = \frac{Eu_r(r,\theta)}{p_o(1+\nu)a} \quad \text{and} \quad v(\rho,\theta) = \frac{Eu_\theta(r,\theta)}{p_o(1+\nu)a}$$

then, by making use of a symmetry argument, it is easily shown that the problem to find K_I and W may be stated as follows:

Solve the dimensionless, plane stress equations of elasticity in the semi-disc $0<\rho<1$, $0<\theta<\pi$ subject to the conditions

i) The stresses and displacements are bounded at r = 0
ii) $s_{\rho\rho}(1,\theta) = s_{\rho\theta}(1,\theta) = 0, \; 0<\theta<\pi$
iii) $s_{\rho\theta}(\rho,0) = s_{\rho\theta}(\rho,\pi) = 0, o<\rho<1$
iv) $v(\rho,\pi) = 0, \; 0<\rho<1$
v) $v(\rho,0) = 0, \; 0<\rho<c$
vi) $s_{\theta\theta}(\rho,0) = -(1 + \log\rho), \; c<\rho<1$
vii) $\lim_{\rho\to 1} \frac{\partial v(\rho,0)}{\partial\rho} < \infty$

By slightly modifying the results in section 2 of Tweed and Rooke (1973) it can be shown that there is a solution of the equations of elasticity, in the given region, which satisfies the conditions (i) through (v) and is such that

$$s_{\theta\theta}(\rho,0) = \frac{1}{\pi}\int_c^1 \frac{P(t)\,M(\rho,t)dt}{\sqrt{[(1-t)(t-c)]}}, \qquad 0<\rho<1 \qquad 3.10$$

and

$$v(\rho,0) = \frac{2}{1+\nu}\int_c^\rho \frac{P(t)\,dt}{\sqrt{[(1-t)(t-c)]}}, \qquad c<\rho<1 \qquad 3.11$$

where $P(t)$ is an arbitrary function of t

and

$$M(\rho,t) = \frac{1}{t-\rho} + \frac{(t^2-1)^2}{t(1-\rho t)^3} + \frac{t(t^2-1)}{(1-\rho t)^2} - \frac{t}{(1-\rho t)} + t - \frac{1}{t} \qquad 3.12$$

It follows that conditions (vi) and (vii) will be satisfied also if $P(t)$ is a solution of the singular integral equation.

$$\frac{1}{\pi}\int_c^1 \frac{P(t)M(\rho,t)dt}{\sqrt{[(1-t)(t-c)]}} = -(1+\log\rho), \qquad .13$$

with subsidiary condition

$$P(1) = 0 \qquad 3.14$$

The stress intensity factor K_I and the crack formation energy W are defined by the equations

$$K_I = \lim_{r\to ac+} \sqrt{2\pi(r-ac)}\,\frac{E}{2}\,\frac{\partial u_\theta(r,0)}{\partial r} \qquad 3.15$$

and

$$W = \int_{ac}^{a} p_o[1+\log(r/a)]\,u_\theta(r,0)dr \qquad 3.16$$

respectively. Therefore, by 3.10 and 3.11 we see that

$$K_I = p_o\sqrt{\frac{2\pi a}{1-c}}\,P(c) \qquad 3.17$$

and

$$W = -\frac{2p_o^2a^2}{E}\int_c^1 \frac{tP(t)\log t}{\sqrt{[(1-t)(t-c)]}}\,dt \qquad 3.18$$

Let K_o and W_o be the stress intensity factor and formation energy respectively of a crack of length 2(a-ac) in an infinite elastic solid, when the crack is opened by a uniform pressure p_o, then after Sneddon and Lowengrub (1969)

$$K_o = p_o\sqrt{\pi a(1-c)} \qquad 3.19$$

and

$$W_o = \frac{\pi p_o^2 a^2}{E}\quad (1-c)^2 \qquad 3.20$$

Therefore

$$\frac{K_I}{K_o} = \frac{\sqrt{2}}{1-c}\quad P(c) \qquad 3.21$$

and

$$\frac{W}{W_o} = \frac{-2}{\pi(1-c)^2}\quad \int_c^1 \frac{t\,P(t)\,\log\,t}{\sqrt{[(1-t)(t-c)]}}\,dt \qquad 22$$

Also of interest is the strain energy release rate $\mathcal{G}_{(\ell)}$ which is defined by

$$\mathcal{G}(\ell) = \frac{\partial W}{\partial \ell} = \frac{1}{E}\,K_I^2 \qquad 3.23$$

where $\ell = a(1-c)$ is the crack length.

If we define

$$\mathcal{G}_o(\ell) = \frac{1}{E}\,K_o^2 = \frac{p_o^2\,\pi a(1-c)}{E} \qquad 3.24$$

then

$$\frac{\mathcal{G}}{\mathcal{G}_o} = \frac{K_I^2}{K_o^2} = \frac{2}{(1-c)^2}\,P^2(c) \qquad 3.25$$

Numerical solutions to equation 3.5 are found by the Gauss-Chebyshev

quadrature technique, Erdogan and Gupta (1972), and the ratio K_I/K_o using Chebyshev-Lagrange interpolation. The Gaussian quadrature formula is used to determine W/W_o.

3.2 EXPERIMENTATION

A pilot scheme was executed to investigate the parameters controlling the design of the self stressed fracture mechanics test-piece. SIC aluminium discs, 3" (7.6 cm) diameter, 1/16" (0.16 cm) thick with a 5^o sector removed, provided the first test-pieces. In practice the sector in the pilot test-pieces was closed by deforming the disc into a cone which, after joining the cut faces, was flattened by clamping between a pair of plattens. The theory demands boundary conditions that naturally set the shear stresses and radial component of stress at the free surface to zero, and that the sector is closed up simply by the $\theta\theta$ component of stress.

These original test-pieces were found to be stressed beyond the elastic limit in some areas of the discs and further aggravation came from buckling. Mitchell and Head (1961) calculated that a disclinated plate will buckle if the angle Ω_{buckle} exceeds 13 (thickness/radius)^2. For the original disc, $\Omega_b = 1^o20'$, therefore buckling presents a problem. It became necessary to optimise the three parameters:

(i) sector cut out angle
(ii) disc radius
(iii) disc thickness.

Variations in (i) and (ii) lead to difficulties in preparing a sound joint and thus, the thickness was increased to 3/16" (0.48 cm) which removes all chance of buckling. The discs could not now be manufactured by punching, each having to be machined, and although this will lead to a more expensive specimen, it should be borne in mind that the test-piece can be used many times as it functions wholly within the elastic regime.

Closing the gap to allow a joint to be made at the cut has been very carefully examined. A custom built chain wrench closes the gap too quickly, and a range of differing gaps were tried to solve the problem. To compensate for the pinching effect a parallel sided cut was effected using a range of gap widths. This reversed the pinching effect in that closure occurred first at the circumference. A series of tests was also carried out where the elastic limit was exceeded and the amount of plastic deformation was monitored. The data from these results allowed the dimensions of a wedge to be determined which would maximize the amount of elastic strain energy stored in the disc, and allow the two faces to close up evenly within the no buckling requirement. The wedge dimensions were

set at 1.1 mm (0.046") at the circumference and 0.75 mm (0.032") at the inner edge, giving a sector angle approximately equal to 1^{o}.

The cleaning process carried out immediately prior to the adhesive joint formation was as follows:

		TIME (mins)	TEMPERATURE (^{o}C)
1.	Chlorinated solvent (carbon tetrachloride)	5	ambient
2.	Non-silicated alkaline cleaner (0.1 molar sodium hydroxide)	10-15	63
3.	Tap water immersion	2	ambient
4.	Tap water immersion	5	38-60
5.	Deoxidiser (170 ml nitric acid 30 ml hydrofluoric acid, 800 ml water)	10-15	ambient
6.	Tap water immersion	2	ambient
7.	Deionised water spray	-	ambient
8.	Phosphoric acid 9-11% by wt in deionised water	-	ambient
	Apply voltage for 1 minute. Step to 10 volts after 2-5 minutes. Maintain for 20-25 minutes		
9.	Tap water spray	10-15	ambient
10.	Deionised water spray	2	ambient
11.	Dry in air	30	80
12.	Cool in air	120	ambient
13.	Prime within 120 min	-	-
14.	Dry in air	30	ambient
15.	Dry in air	60	123

The cleaned aluminium test discs had the epoxy resin strip or layer of paste positioned between the opposing faces of the wedge cut out, with restraining plates on each side of the discs to maintain flatness during the closing operation. Standardisation was achieved using a torque wrench set at 16 ft-lb. Immediately on closure, the restraining plates were removed and the prepared joints gelled and cured. The manufacturer's data sheets were strictly followed for both cure times and temperatures. Examination of the joints revealed reasonable reproduction of the bond line thickness, approximately the thickness of the resin strips used, 0.25 mm. The proprietary adhesive resin film most extensively employed was FM73M, but others which were tested in the experimental programme were Redux312/5, and DLS468/DLS476.

The length of crack when present, was measured and the disc was then immersed in boiling water for varying periods of time. After each immersion the length of crack was measured. This process was repeated until the crack had propagated the full length of the glue line, with frequent water changing to avoid contamination. On examining the crack it was always found that the crack length was different when viewed from the two sides of the disc. For the purpose of evaluation, the average value of the crack length read from both sides was noted. Also, near the crack tip it became increasingly difficult to distinguish where the crack actually finished, a result of the hairline nature of the crack. When the crack length was apparently shorter in the glue line after further boiling, the length of crack was taken to be the distance to the end of the last crack. With some discs that did not initially crack on release of the clamp an attempt was made to induce a starter crack in the glue line by either sawing a small nick at the periphery of the joint, or by immersing the discs in liquid nitrogen to increase the stress field in the disc by contraction of the aluminium. Unfortunately, neither method proved to be successful.

A series of experiments were performed using a perspex disc of similar dimensions to the aluminium specimens. The object here was to use a photoelastic method to study the stress field during crack growth. Initiation of the crack has proved difficult and satisfactory monitoring of the stress field during propagation is presently under study.

Two undergraduate students, Gilbert and Longden, working here in Bristol have become particularly interested in the experimental evaluation of the fracture mechanics test-piece and are taking this piece of interesting research a stage further.

3.3 RESULTS AND DISCUSSION

On release of the chain-wrench clamp from around the stressed disc, crack lengths vary according to the epoxy resin adhesive formulation used to make the joint. The crack always propagates the full glue-line length ($l/a = 1$) for resin Redux 312/5, whereas for FM73M no crack is present in the joint ($l/a = 0$). The l/a values obtained for DLS468/DLS476 are 0, 0, 0, 0.40 and 0.82.

Correlation of crack length with independently measured values of $\mathcal{G}_{IC}$ is required in order to generate calibration curves for a given geometry of self-stressed disc. Available $\mathcal{G}_{IC}$ data for the dry adhesives show variations, e.g. FM73M has values of 2.38 kJ/M^2 and 3.67 kJ/M^2 for two different batches. Redux 312/5 and DLS468/DLS476 both have $\mathcal{G}_{IC}$ values of 2.8 kJ/M^2. Using as calibration points, the $\mathcal{G}_{IC}$ values for dry FM73M and Redux 312/5 and the stable crack lengths measured after mechanically introducing started cracks, two values of l/a measured for DLS468/DLS476 indicate that $(\mathcal{G}_{IC})_{max}$ is 3.65 + 0.55 kJ/M^2.

Conflict evidently exists between the published data and the results obtained here; with DLS468/DLS476 our self-stressed discs were found to crack partially or not at all. With Redux 312/5, the bonds crack over the full length of the glue line. With FM73M no cracks are found suggesting that $\mathcal{G}_{IC}$ is greater than 2.8 $kJ.M^2$. With a view to clearing up this dilemma, independent measurements of $\mathcal{G}_{IC}$ on the particular batches of adhesive films used here are being made at the University of Cambridge.

Results presenting the variation of $\mathcal{G}_{IC}$, expressed as a fraction of $(\mathcal{G}_{IC})_{max}$ with water uptake by FM73M are shown in Figures 12 to 15. The specimens were immersed in boiling distilled water. The time for the starter crack to appear varied from 5 to 130 mins. Examination of the joints after total failure show that propagation of the cracks occur through the resin and definitely not at the resin/aluminium interface.

4. PHOTOELASTIC IMAGING OF DEFECTS

Andrews and Wallis (1977) were first to demonstrate that a light emitting diode(LED) can be used to illuminate the stress waves travelling in a visualizing block when viewed through crossed polars. The method was applied to the detection of defects in opaque solids by Hardy, Turner and Ashbee (1978). There is a strong reflected component, mode converted, from a defect which can be observed some distance from the flaw, after the stress wave has travelled from the specimen into the transparent block. This wave interacts with direct waves from the transducer to give interference patterns for which a computer model has been devised by Kitson, Low and Turner. All the longitudinal and shear waves emanating from the transducer, the interface and the defect, with and without mode conversion, are investigated.

4.1 COMPUTER MODEL

Figure 16 shows the representation of the model, with a series of radiating point sources depicting the transducer. An array of points P(x,y) forms the visualized zone and was originally set at 31 x 31 to conform with computer graphics. It is assumed that the defect is perfectly round, that longitudinal (L) and shear (S) waves emanate from the transducer point sources, and that on reflection and refraction both mode converted and unconverted waves emerge. The following relationships hold:

$$\frac{\sin\beta}{V_L} = \frac{\sin\alpha}{V_S}, \qquad \frac{\sin\gamma}{V_S} = \frac{\sin\delta}{U_S}$$

where V_L and V_S are the velocities in the specimen and U_S the shear velocity in the visualizing quartz. Note that the subscripts are inter changeable for the incident shear wave reflected as longitudinal and for a refracted longitudinal wave. Relative intensities may be evaluated using the Zoeppritz equations and an attenuation factor of $1/\sqrt{x}$ is included for the wave amplitude as it travels away from the source. Hence we may find the exact path which any particular ray travels together with its amplitude at a point. Each flash of the LED is represented by a sine wave, singly for single flash and several cycles for multi-flash.

The complete picture is built up as follows: each type of wave [longitudinal/shear (LS), long/long/shear (LLS), etc.] is considered in turn for each transducer point source. The program calculates (i) the path between the transducer point and a point in the rectangular visualized array (subject to the path being possible, (ii) when the sound pulse arrives at the visualizing point, and (iii) the amplitude. The

amplitude is then multiplied by the value of the illumination waveform at that specific time, and repeated for all the points in the rectangle. Results for all the transducer elements are superimposed, and finally the whole process repeated for each wave type in order the simulate the complete interference pattern. The final array is normalized to give the negative or compressive regions the lighter shades of the computer simulation and the positive or tensile regions the darker areas: a normalization analogous to the quarter wave plate.

Two main calculation procedures are used in the program, REFPATH and DIRCALC. REFPATH, the flow diagram is shown in Figure 17, deals with the patterns resulting from the wavetypes which are reflected from the defect, whilst DIRCALC handles those direct from the transducer. Any wavetypes can be included, but it is found experimentally that many are of little importance and only LLS, LS, and SSS need to be considered. It should be remembered here that the experimental arrangement of the photoelastic method helps enormously to reduce the number of wavetypes which contribute to the visualization. In the direction of principal stress, i.e. the direction of the stress wave propagation, 45 degrees to the polar axes, only longitudinal waves are visualized, and at 45 degrees to this direction, along the polar axes, only transverse waves can be seen. It is in this direction, along the polar axes that we are primarily concerned as it is here that most information is displayed.

The first attempts to display the visualized array by computer graphics took advantage of SYMAP [SYMAP is a computer program for producing maps which graphically depict spacially disposed quantitative and qualitative information. SYMAP was designed and developed by the Laboratory for Computer Graphics at Harvard University, USA] and then SYMVU was employed to give a topographical representation of the data. The former program has the advantage that direct comparisons could be made of the photographic results, but suffered from having only ten levels of shading, whereas the latter shows the dislocations very well. Figure 18 shows the contour map where the maximum pressure is represented by a height of 3 ins, with a minimum of 0 ins. The viewing point is at an altitude of 30 ins with an azimuth of 335 degrees. Dislocations in this context refer to the line of discontinuities in wavefronts which line runs in the direction of the stress propagation. A new program was written therefore, following the principles of SYMAP, but with facility for 100 shadings. Some time was spent experimenting with different overprinted characters in order to get a set of evenly varying shades. It was found that a sub-routine designed to interpolate the brightness between the array points gave a smoother picture when the visualization density map was plotted on the line printer.

4.2 VISUALIZED SOUND EXPERIMENTS

Figure 19 shows a schematic diagram of the apparatus. The LED sends a single pulse (single flash) or flashes a number of times in synchronisation with the ultrasonic frequency (multi-flash) to illuminate the stress field in the quartz visualizing block. The birefringence exhibited by quartz when it is stressed, results in a small component of light being propagated perpendicular to the axis of the polarizer to give elliptically polarised light. This contrasts with transmission of the illuminating pulses through unstressed regions of the quartz since here the light remains plane polarised. The analyser, set at 90 degrees to the polarizer, permits transmission of the small component only so that the stressed regions are revealed as bright fringes. Bright fringes arise in both tensile and compressive regions, and, by suitably setting the quarter wave plate, all the light from the most highly compressed region can be eliminated. Thus some light can be seen for unstressed regions with the tensile areas brighter still, the whole picture being built up stroboscopically at repetition rates up to 3 kHz. Full details of the experimental approach are given in Hardy, Turner and Ashbee (1978).

The experiments which have been carried out in parallel with the computer modelling have been mostly single flash, i.e. a single LED pulse for illumination. Single flash images are difficult to record because they are so dim, but it is necessary to identify the different wavetypes. A series of experiments were conducted with no specimen in place in order to investigate the transducer for accurate computer modelling. For these, three flashes were used. As the shear waves travel more slowly than the longitudinal waves, the shear fringes are closer together: a fact which with their position simplifies the identification of any particular wave. To investigate the transducer beam, a series of photographs was taken varying the polar axes, thus compensating for the angular sensitivity of the optical arrangement. The angular spread of the beam was found to be approximately 90 degrees.

A number of different transducers have been tried including two commercial designs, but the results have been obtained with a transducer designed and built in the laboratory. It consists essentially of a brass plate 0.9 ins. (2.2 cm) diameter and 5 λ /4 thick on to which a 0.4 in. (1.0 cm) diameter piezo-electric disc is soldered. However, the image is still complicated by secondary waves arising from reflections within the brass and disc.

After the initial experiments it appeared that two wavetypes were contributing to interference patterns seen in the visualized region. Firstly, the wave reflected from the defect. This is mode converted but

crosses the interface between specimen and visualizing block without a further conversion (LSS). Secondly, the direct wave originating as shear at the transducer and again crossing the interface without mode conversion (SS). The experiments show, however, that the prominent shear waves leave the specimen/quartz interface at roughly the same time as the primary longitudinals. To investigate this further, the positions of the primary longitudinal and shear waves were plotted for a series of different delay times. Different specimen thicknesses were used for the measurements as well as readings taken without a specimen. The results shown in Figure 20 strongly suggest that the shear waves arise by way of mode conversion at the interface, having crossed the specimen as longitudinal waves. Shear waves generated from the transducer are apparently unimportant. Different effects of the quarter wave plate on the two wavetypes account for the incorrect positioning of the specimen/quartz interface in that Figure.

To establish a baseline from which to judge images from resin specimens a range of steel specimens have been produced with thicknesses up to 1 1/4 ins (31.2 mm) each containing a transverse hole 'defect' having diameters in the range of 0.04 ins (1 mm) to 0.4 ins (10 mm). A 35 mm Nikon F2 photomic camera is used to record the results with an eight minute exposure on ASA 400 film for single flash at different delay times.

The delay time is measured from the original ultrasonic pulse to the LED flash, and is the time taken for the sound to travel from the transducer to the visualized position. The TTL control enables this to be accurately measured, since the delay monostable and thyrister fired ultrasonic wave are triggered by the same pulse. A digital readout of the delay is used which can be checked against the time base of the oscilloscope.

4.3 RESULTS AND DISCUSSION

The results are presented in a graphical form which show both experimental position and the computer simulation. Figures 21 and 22 show the results for two delays, 8.8 and 13.4 s respectively for steel specimens. The dotted lines give the position of the computer prediction and the hard lines have been traced from the photograph. They show that the program correctly predicts the wavefront spread for both the LSS and LS waves. It is the former which represents 'information' from the defect. Differences in the lengths of the wavefronts can be attributed to the differences in the transmission coeffecients. The latter are complicated by the acoustic coupling at the specimen/quartz interface by a thin film of water. Broadening of the lower LS wave is caused by the superposition of the LLS wave i.e. the reflection from the hole without mode conversion.

The experimental delay times against the theoretical time required to align the LS waves is shown in Figure 23. The gradient of unity within 3% demonstrates further that the program correctly predicts the LS position.

A sequence of tests was undertaken with thicker specimens 1 1/4 ins (31.2 mm) containing a hole 0.3 ins (8 mm)diameter, where the distance between the hole centre and the transducer, A, was varied. Figures 24, 25 and 26 give the results for A = 0.27 ins (7 mm), 0.61 ins (15.6 mm) and 0.95 ins (24.2 mm) respectively.

The above results refer to single flash which was regarded as the best approach for wave indentification, whereas the original approach began with multiflash. More information is carried in the multiflash pictures as the close up of the interference patterns from 0.04 in (1 mm) radius 'defect' shows in Figure 27. The multiflash simulation of Figure 28 illustrates the interaction of the LS wave and the LSS wave reflected from a hole of 0.04 ins (1 mm) radius.

In composite materials it has been possible to calculate both longitudinal and shear wave velocities by measuring the delays across a known specimen thickness. Velocity variations have been detected during water uptake and are attributed to resin plastication and to post curing. Experiments on composite laminates containing holes have been less successful. Attenuation of the wavetypes is more marked, and the shear wave rapidly loses energy as it proceeds across a series of interfaces. The problem is aggravated by higher frequencies, resolution of the fringes being impossible at frequencies in excess of $\sim$10 MHz.

REFERENCES

Alfrey T, Gurney E F and Lloyd W G (1966) J Polym Sci C12, 249

Andrews D R and Wallis L J (1977) Light emitting diode as a short duration stroboscope-application to visualization of ultrasound. J Phys E 10, 95

Barrer R M (1941) *Diffusion in and Through Solids*, Cambridge University Press, Cambridge 1941

Bearman R J and Kirkwood J C (1958) J Chem Phys Vol 78 No 1, 136-145

Crank J S and Park G S (1968) Eds Diffusion in Polymers (Academic Press London)

De Groot (1951)

Erdogan F and Gupta G D (1972)

Eshelby J D (1966) Brit J Appl Phys 17, 1131-1135

Farrar N R and Ashbee K H G (1978) J Appl Phys 11, 1009-13

Farrar N R, Turner T W and Ashbee K H G (1979) The physical mechanisms responsible for deterioration in the properties of composite materials. Proceedings of the Third International Conference on Mechanical Behaviour of Materials, Cambridge.

Frisch H L, Wang T T and Kwei T K (1969) J Pol Sci 7 A-2, 879

Gutfield R J von and Melcher R L (1977) Appl Phys Lett 30, 257

Hardy G J, Turner T W and Ashbee K H G (1978) Detection of defects in opaque solids using visualized ultrasound. Metal Science 12, 406

Kitson N K, Low S A and Turner T W (1979) "Photoelastic visualisation experiments and a computer model for non-destructive testing". Ultrasonics International 79 Conference, Graz, Austria

Kwei T K and Zupko N M (1969) J Pol Sci A-2, 7, 867

Mitchell J H (1899) Proc Lond Math Soc 31, 100

Mitchell and Head (1961)

Prigogine I and Nicholis G (1967) J Chem Phys USA Vol 46 No 9 3542

Sargent J P and Ashbee K H G (1980) J Adhesion

Sargent J P and Ashbee K H G (1980) Polymer Composites (In press)

Slater E A, Baborovsky V M and Marsh D M (1975) Proceedings of the Ultrasonics International Conference

Sneddon I N (1945) Proc Roy Soc Lond A187, 65-73

Sneddon I N and Lowengrub M (1969) Crack Problems in the Classical Theory of Elasticity. Wiley J and Sons NY

Tweed J and Rooke DP (1973) Int J Engng Sci 11, 65-73

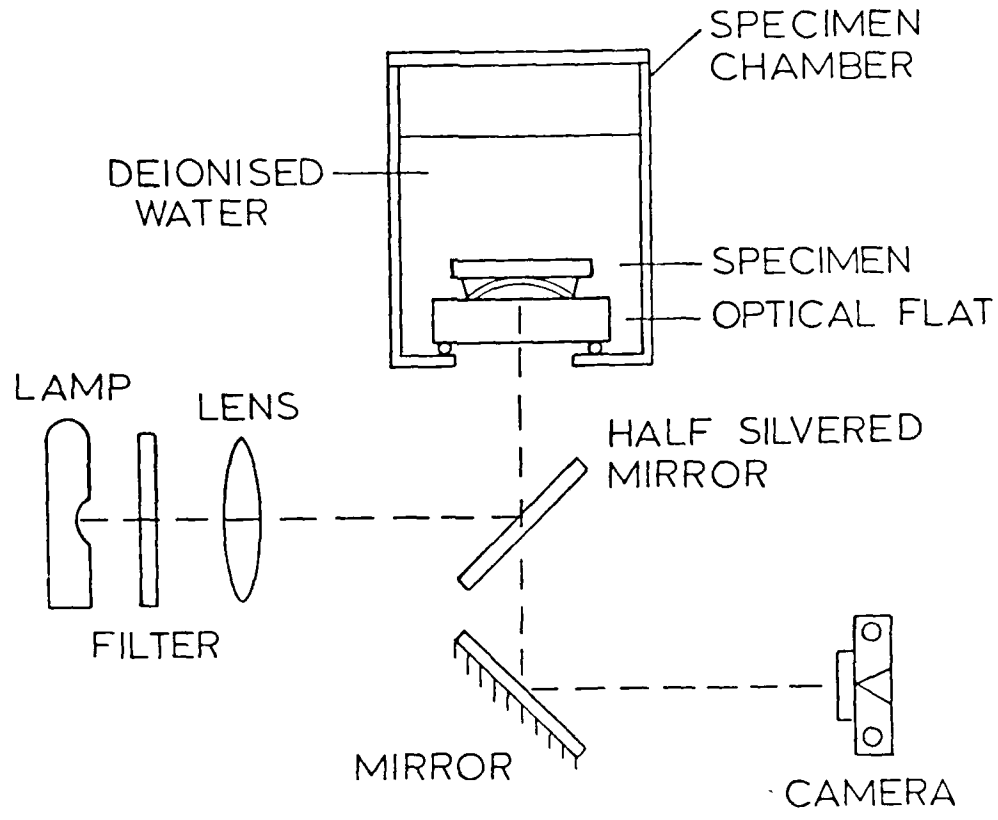

Figure 1. Experimental arrangement of Newton's rings apparatus.

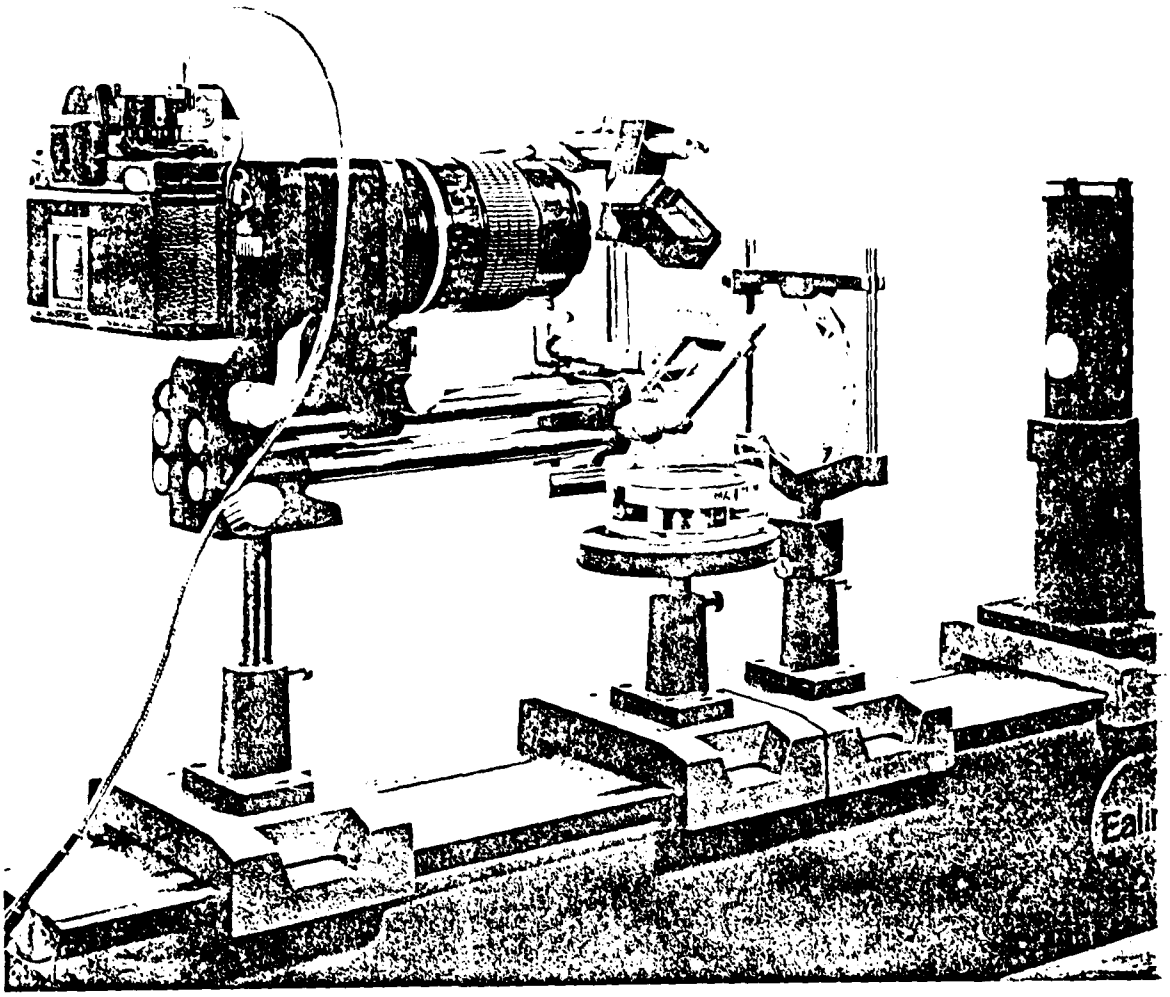

Figure 2. General view of ambient temperature apparatus.

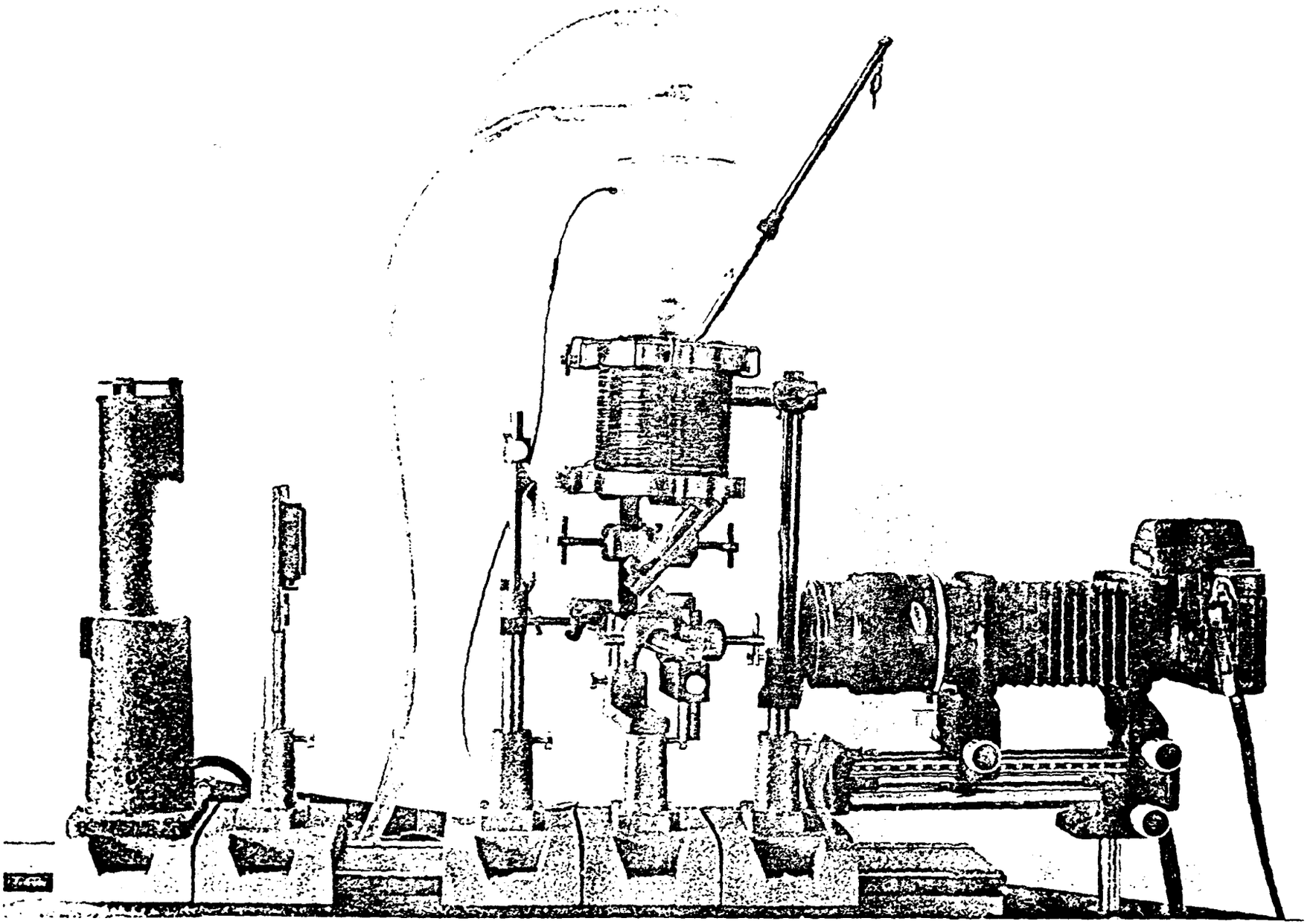

Figure 3. High temperature (<100°C) apparatus.

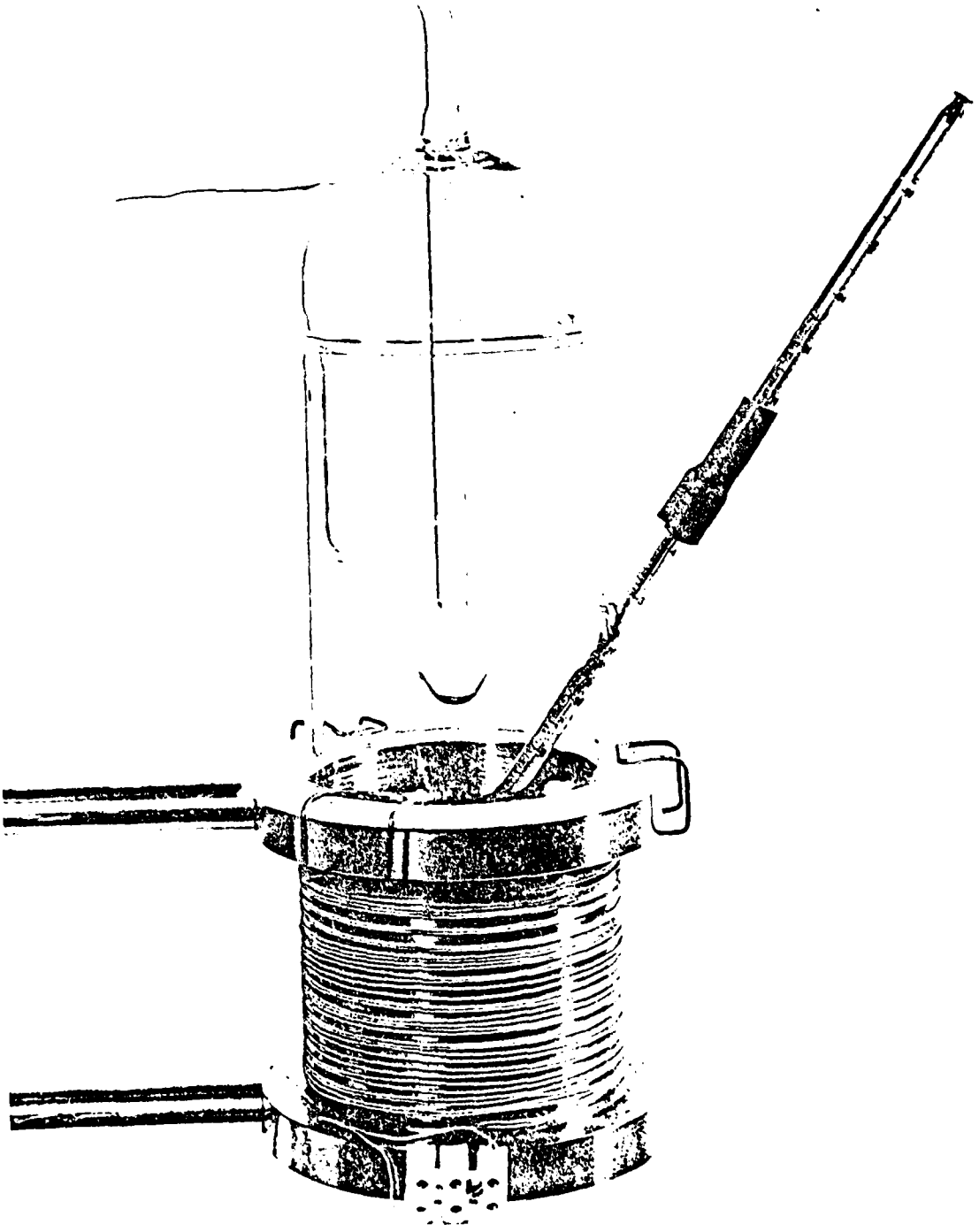

Figure 4. Mark II hot water apparatus.

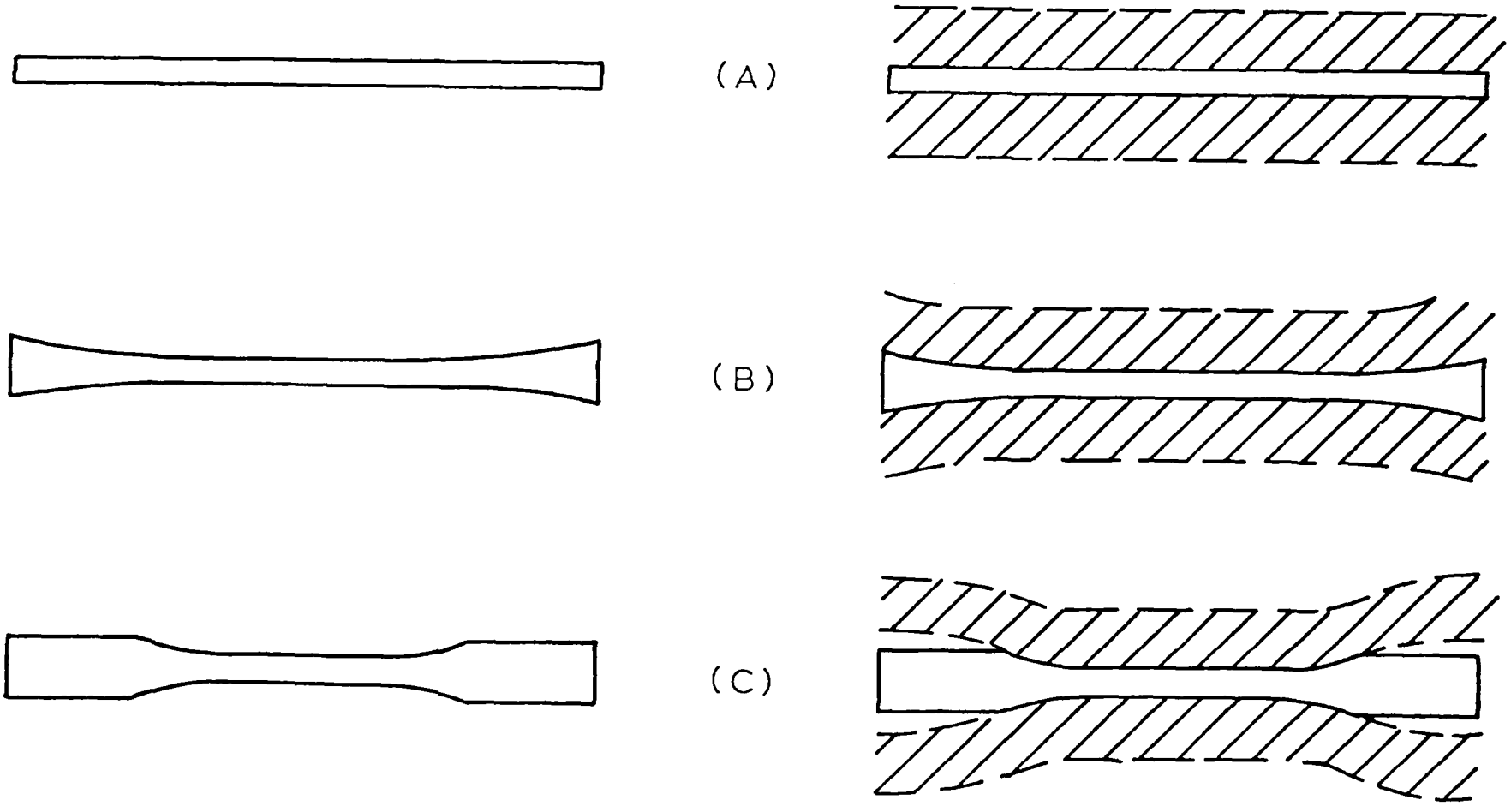

Figure 5. Inhomogeneous swelling associated with water uptake.

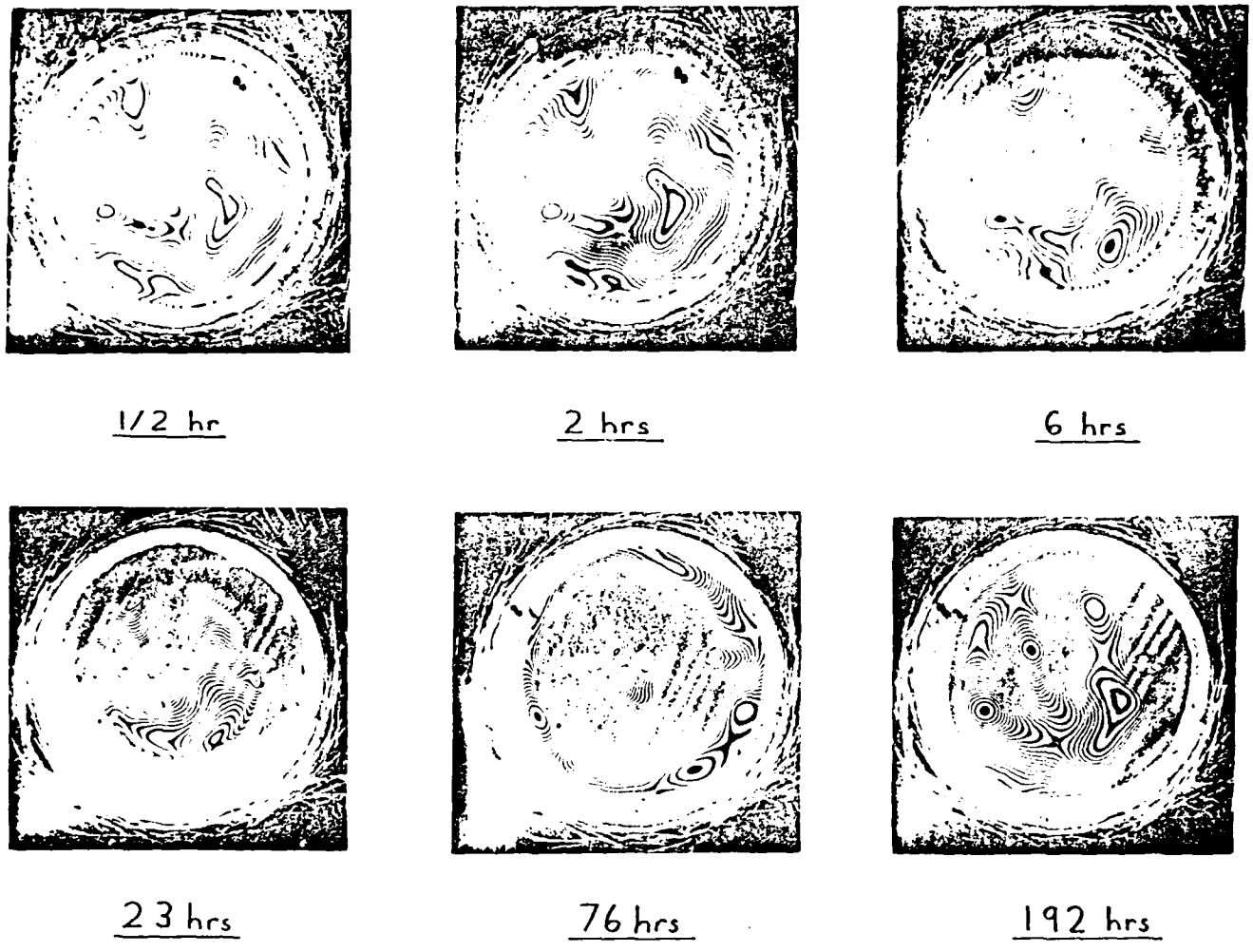

Figure 6. Sequence of interference patterns showing the swelling and debonding of FM 1000 *epoxy resin film adhesive* during immersion in water at 80°C.

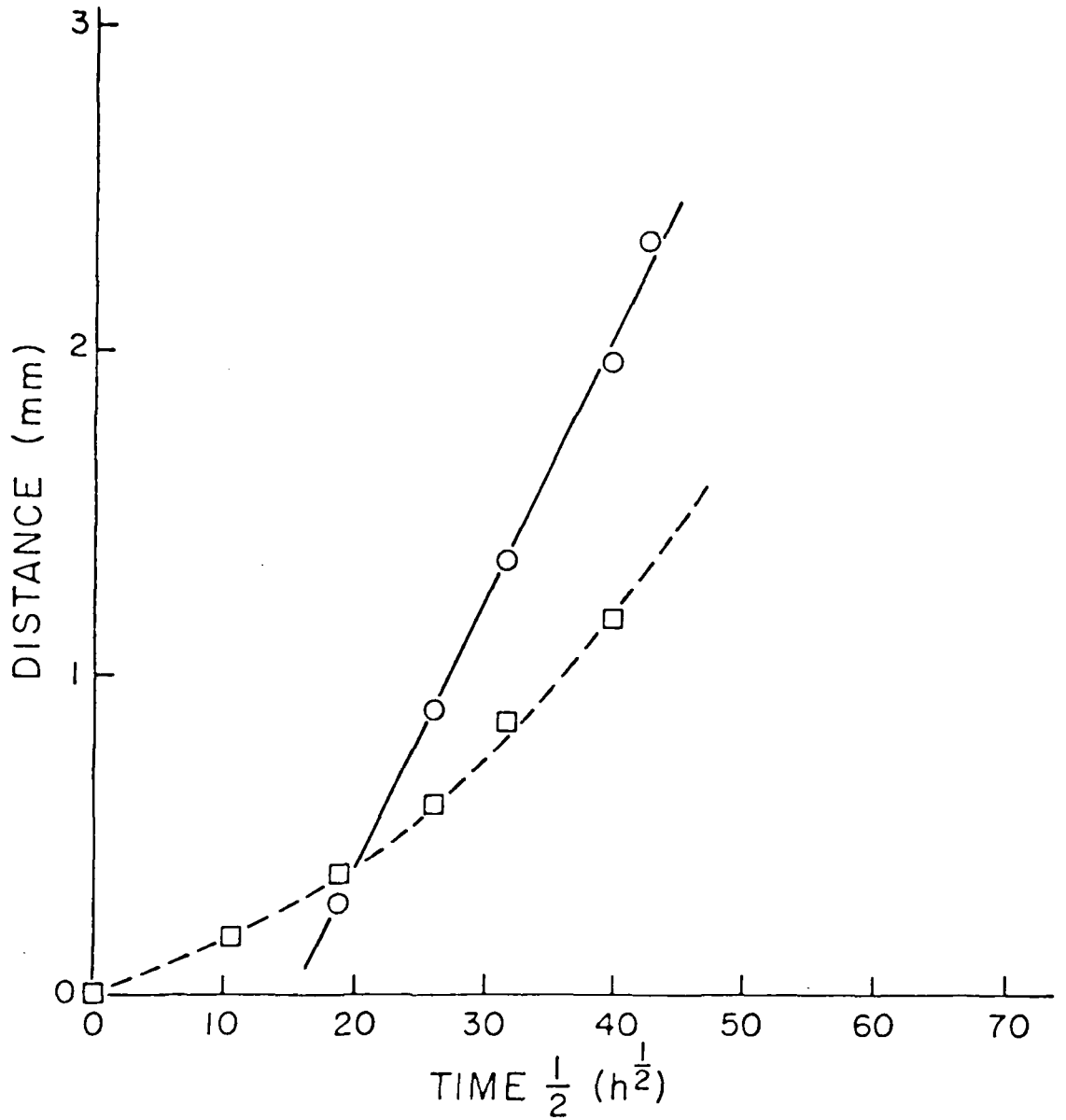

Figure 7. Migration of the shoulder in a Newton's ring (□) and of a point on the debonding crack (○). 20°C water.

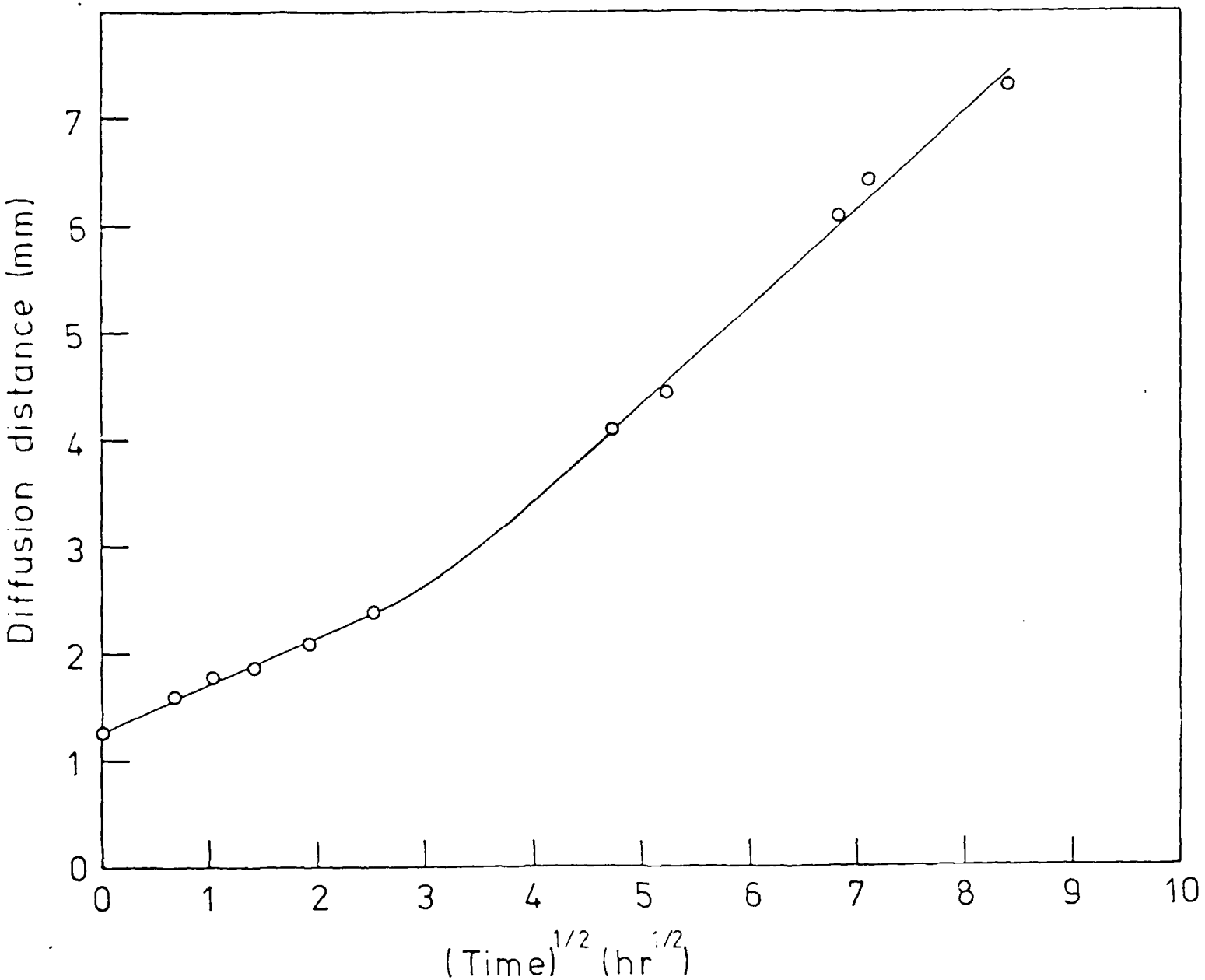

Figure 8. Diffusion rate for an FM 1000 adhesive joint between anodized titanium and glass cover slip.

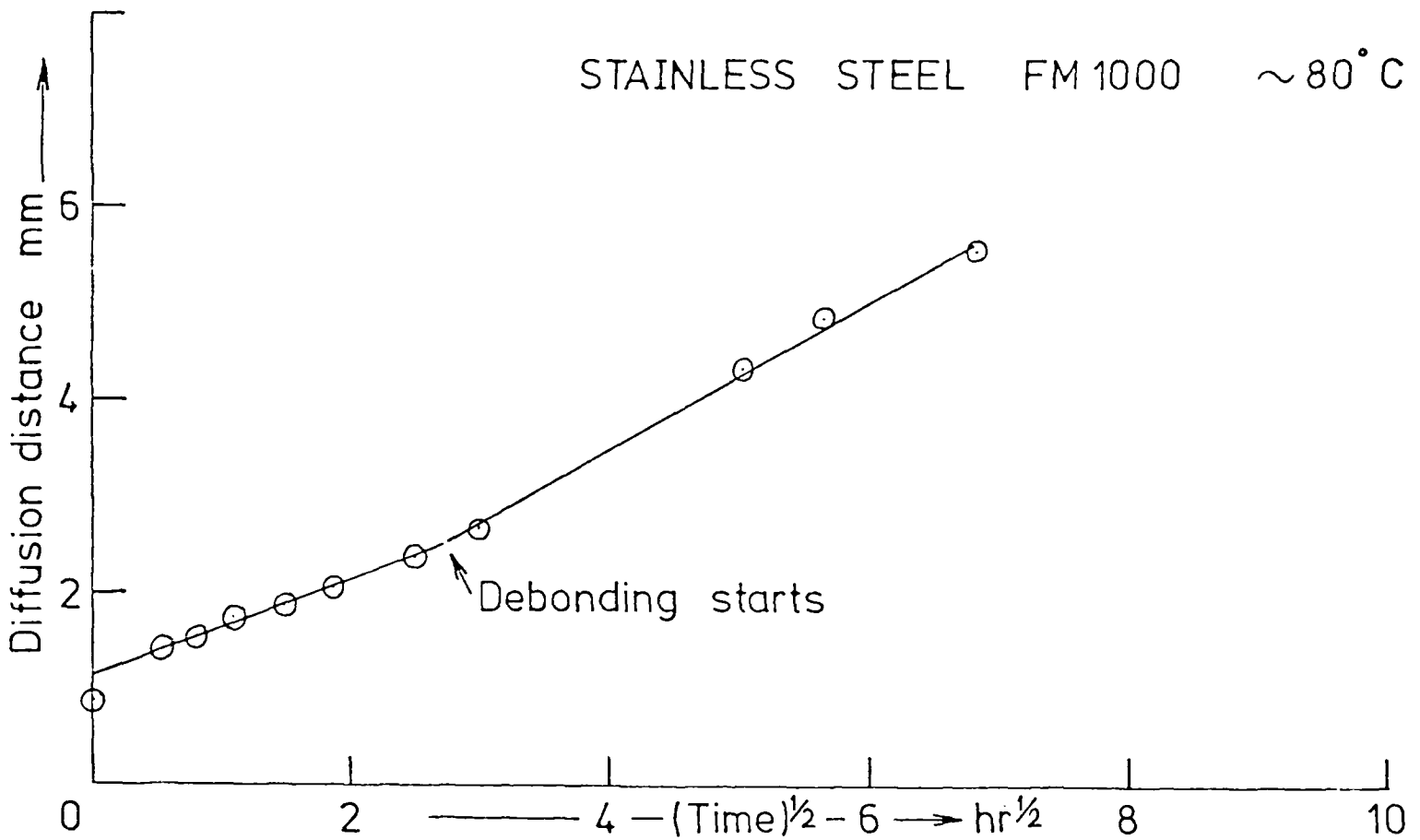

Figure 9. Diffusion rate for an FM 1000 adhesive joint between stainless steel and glass cover slip.

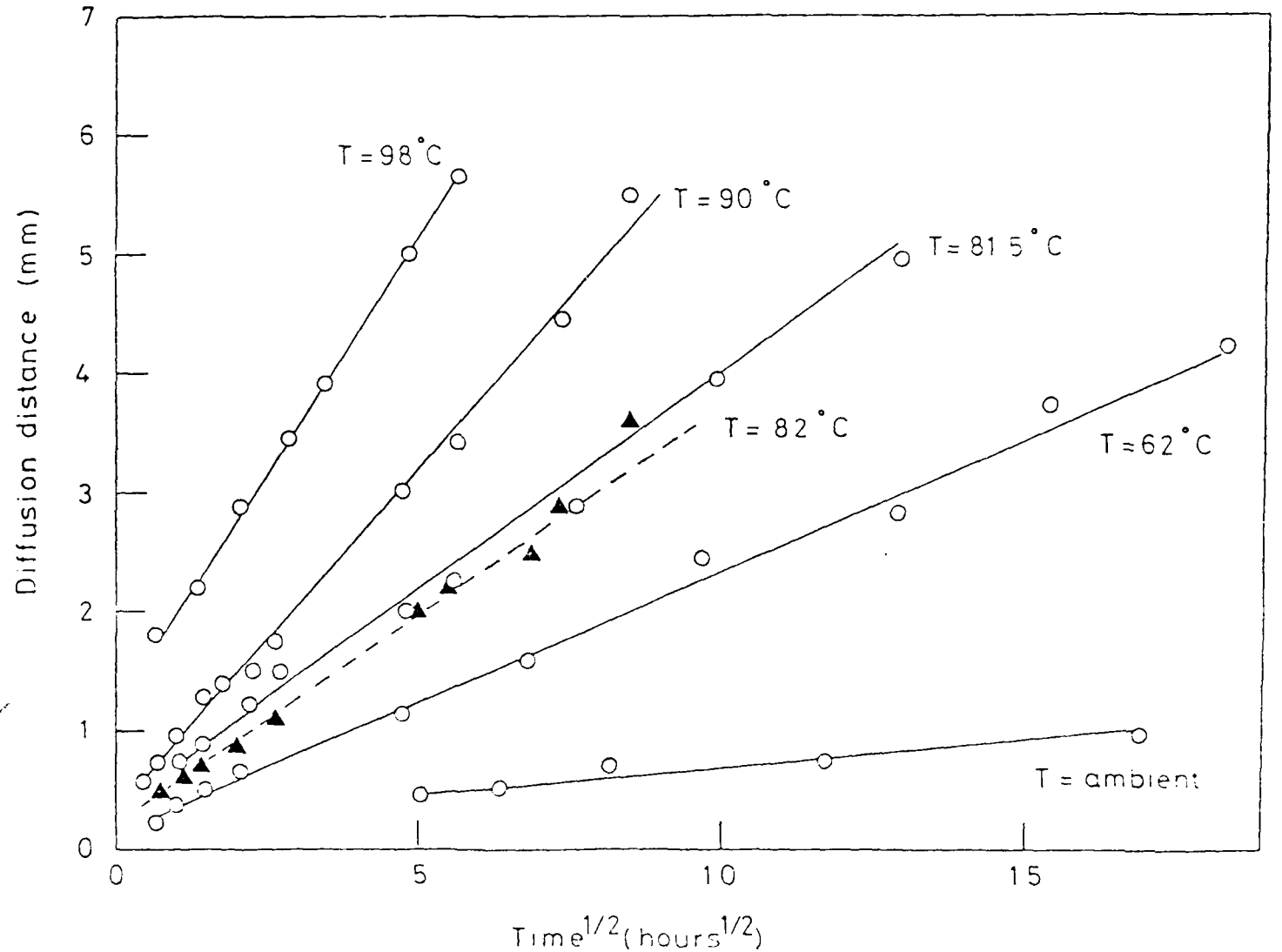

Figure 10. Migration distance of the 1st Moiré fringe for Redux 312/5 ○, and FM 73M ▲, against the square root of time.

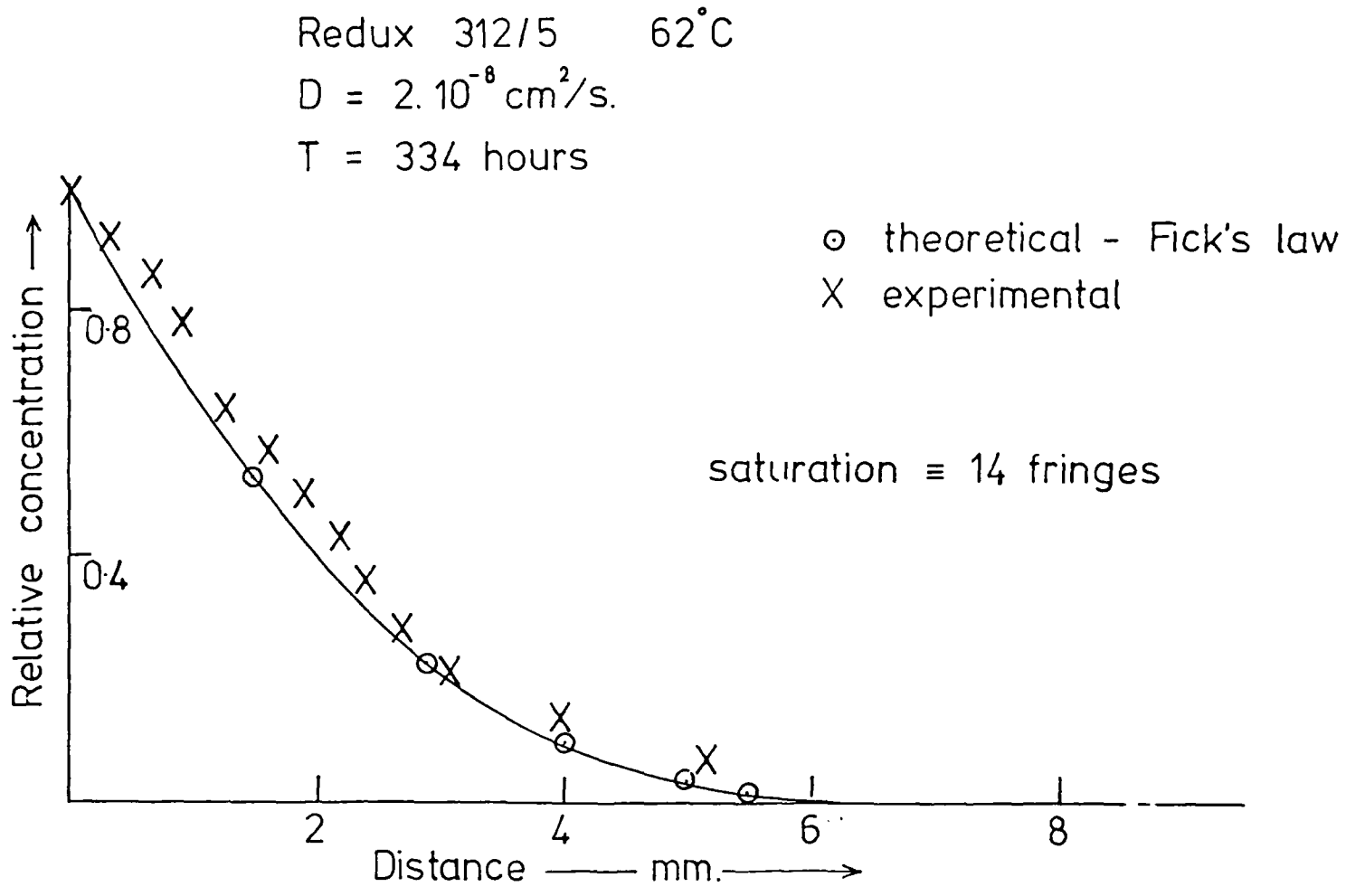

Figure 11. Graph showing the relative concentration across one diameter of a model adhesive joint.

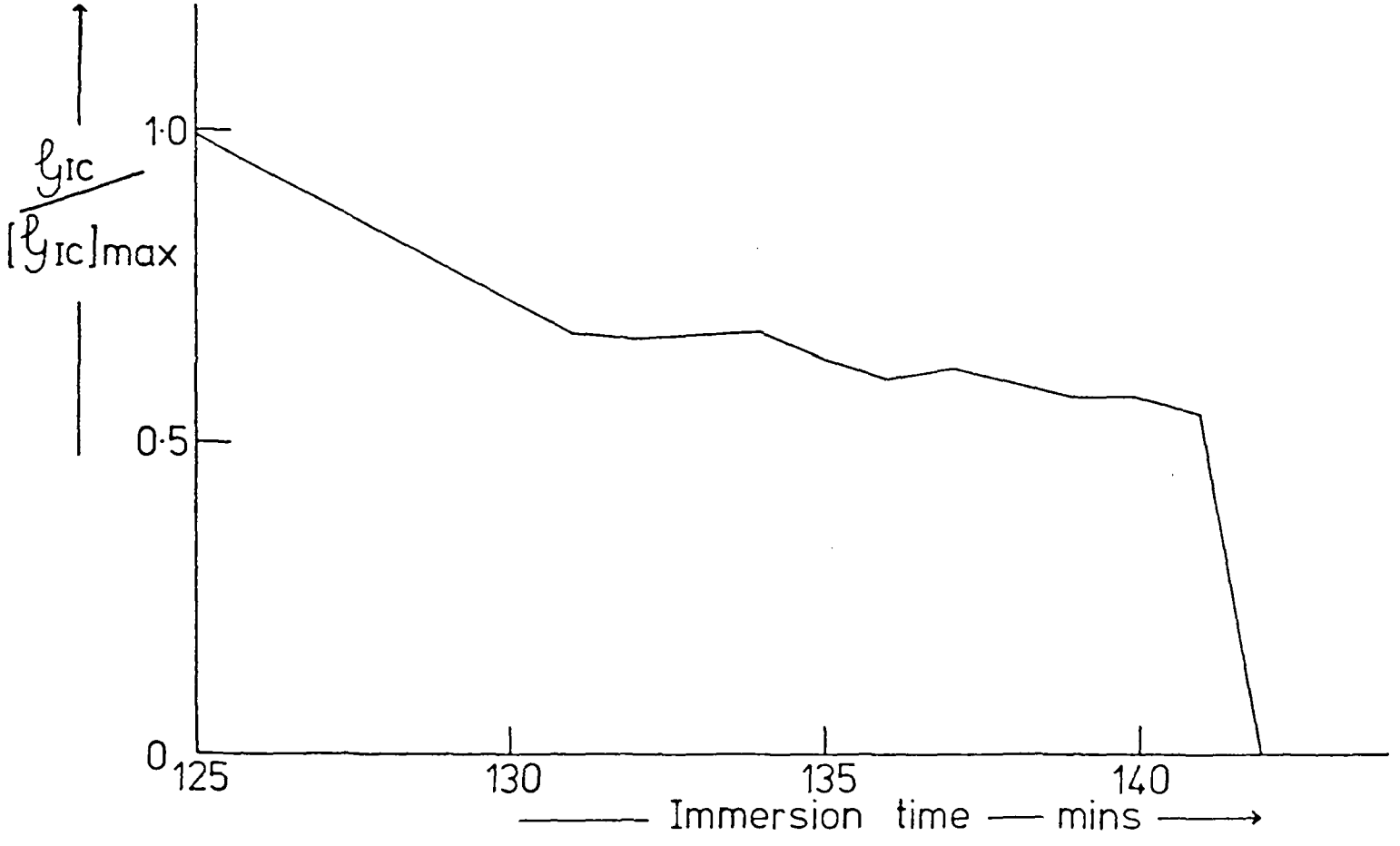

Figure 12. Plot of $\mathcal{G}_{IC} / (\mathcal{G}_{IC})_{max}$ - specimen A.

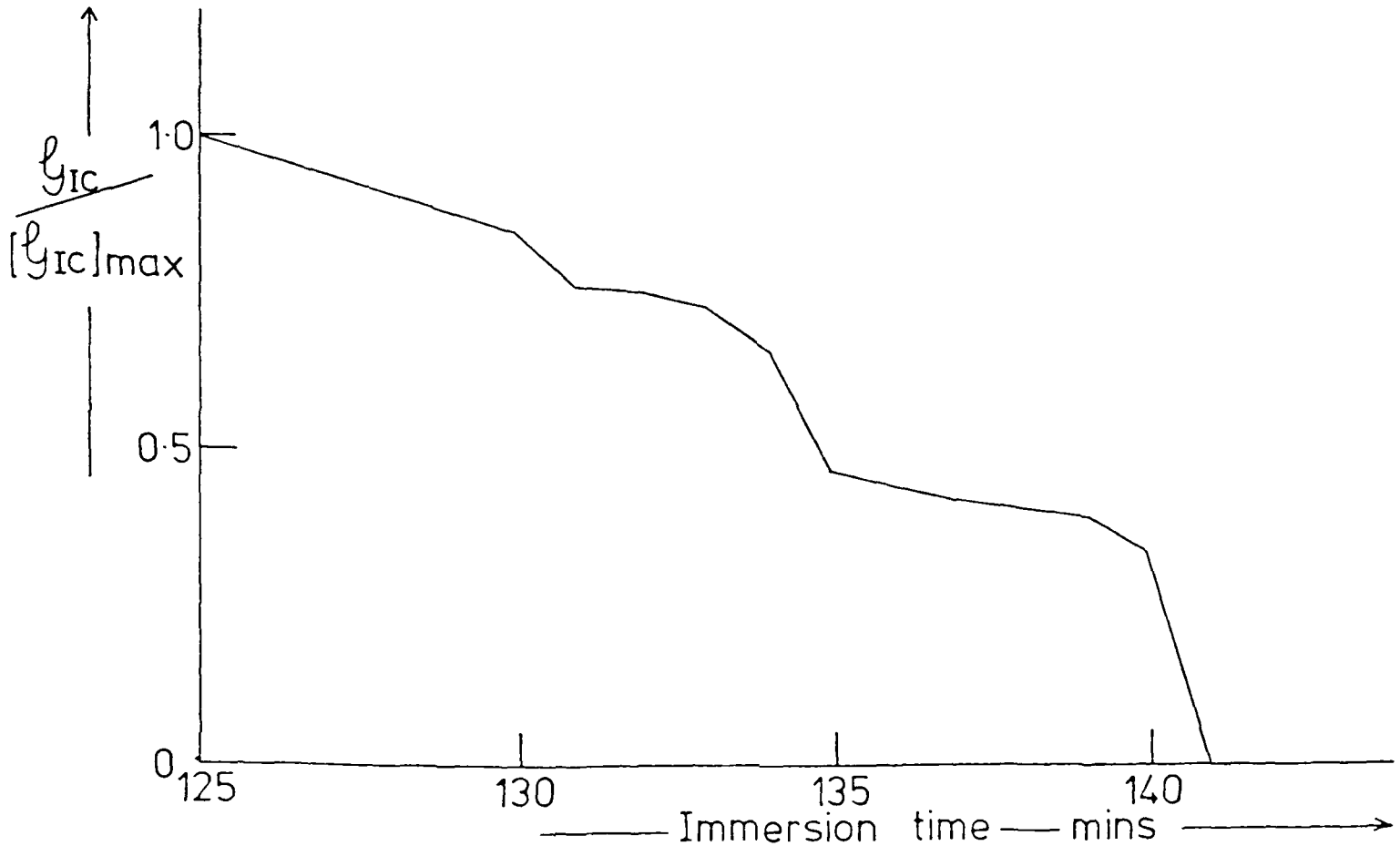

Figure 13. Plot of $\mathcal{G}_{IC} / (\mathcal{G}_{IC})_{max}$ - specimen B.

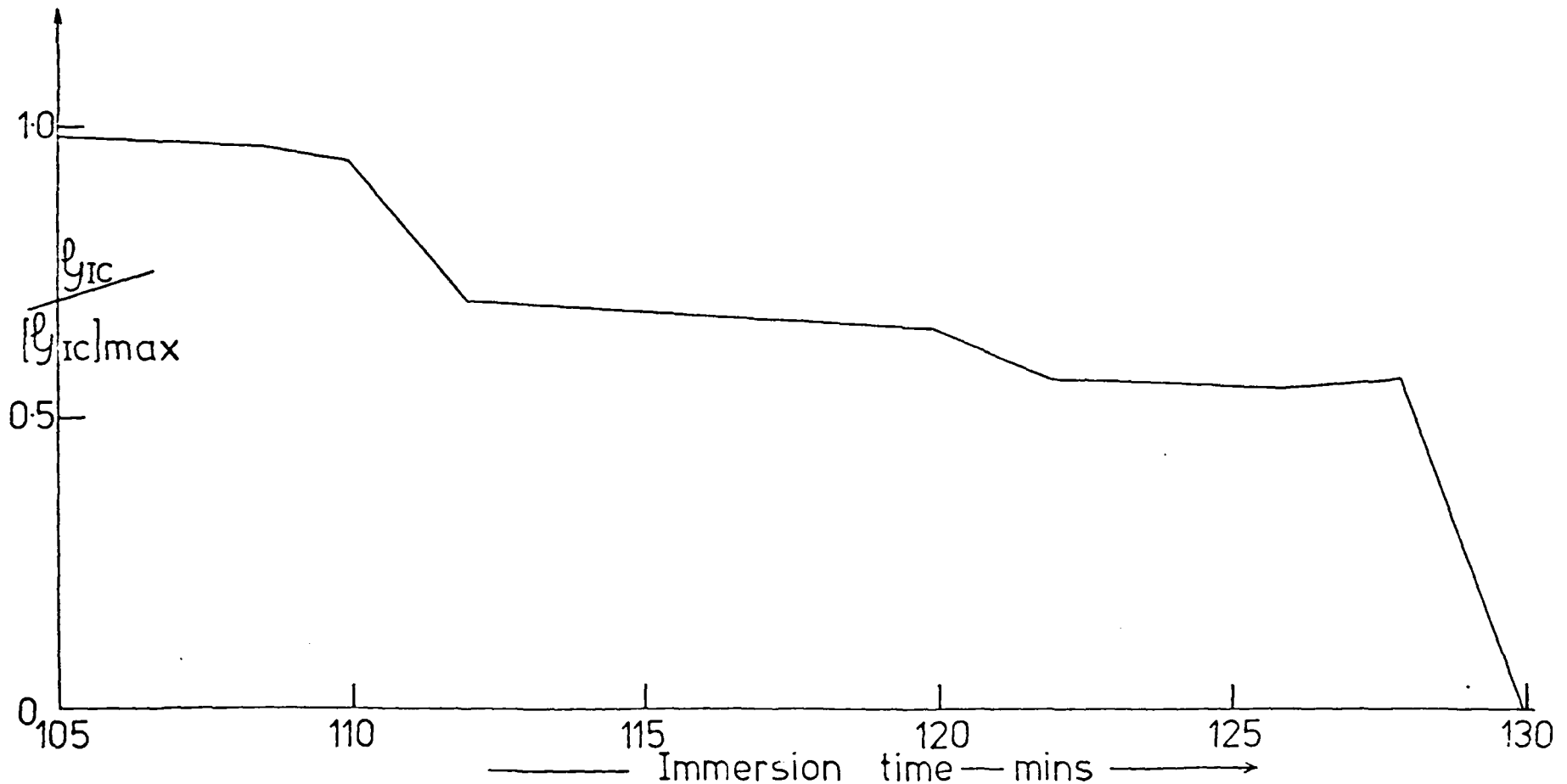

Figure 14. Plot of $\mathcal{G}_{IC} / (\mathcal{G}_{IC})_{max}$ - specimen C.

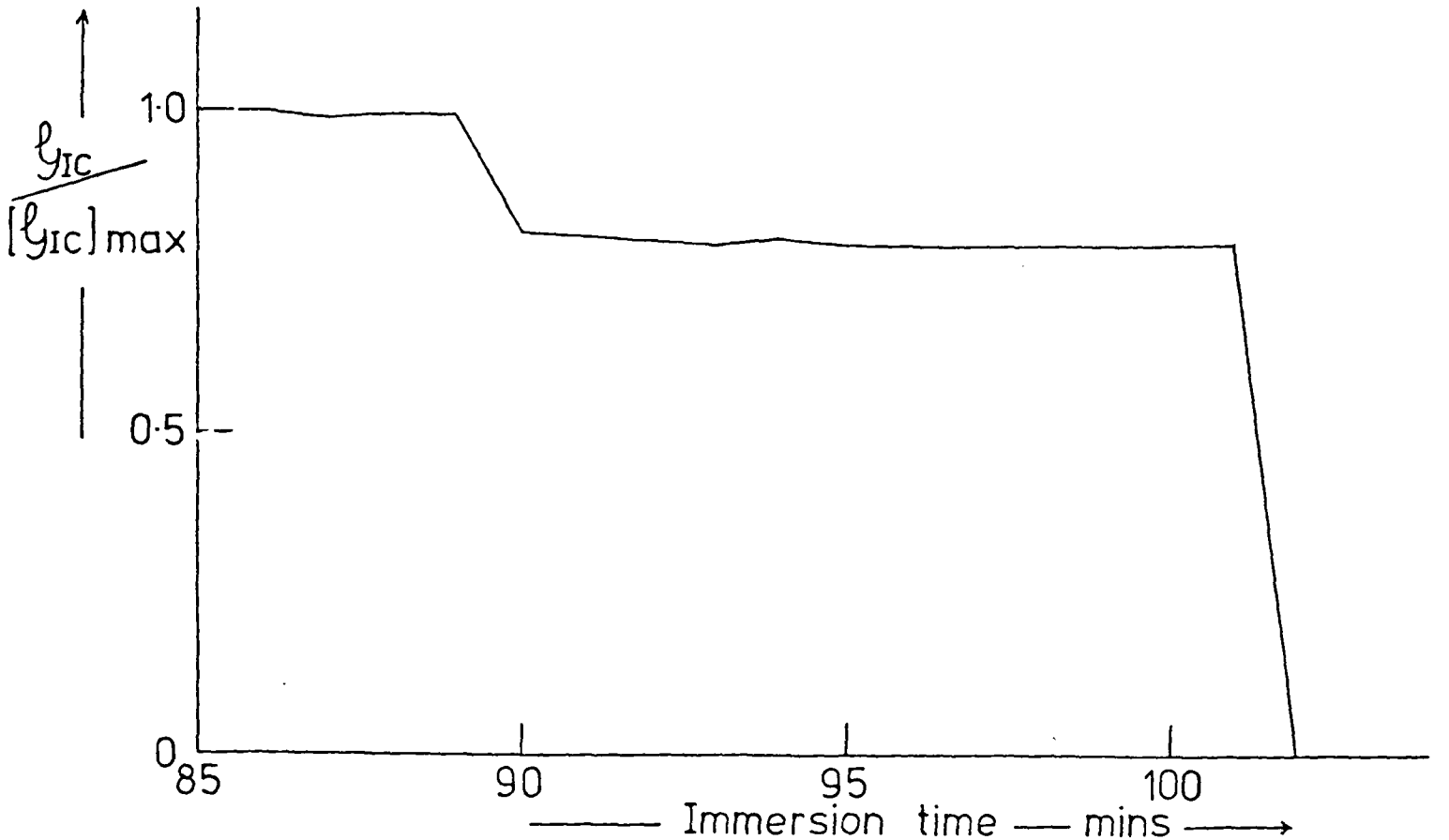

Figure 15. Plot of $\mathcal{G}_{IC} / (\mathcal{G}_{IC})_{max}$ - specimen D.

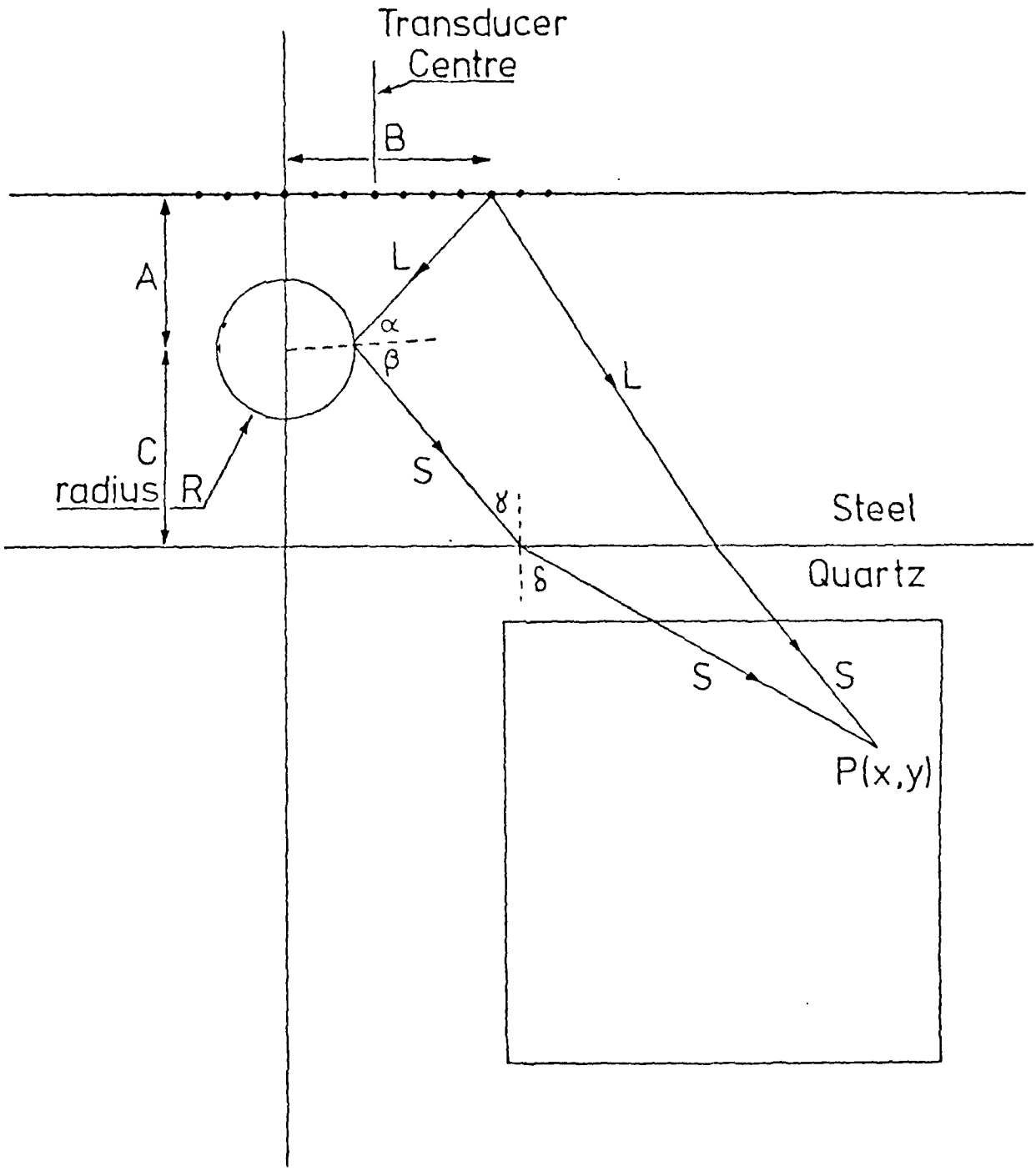

Figure 16. Computer model representation.

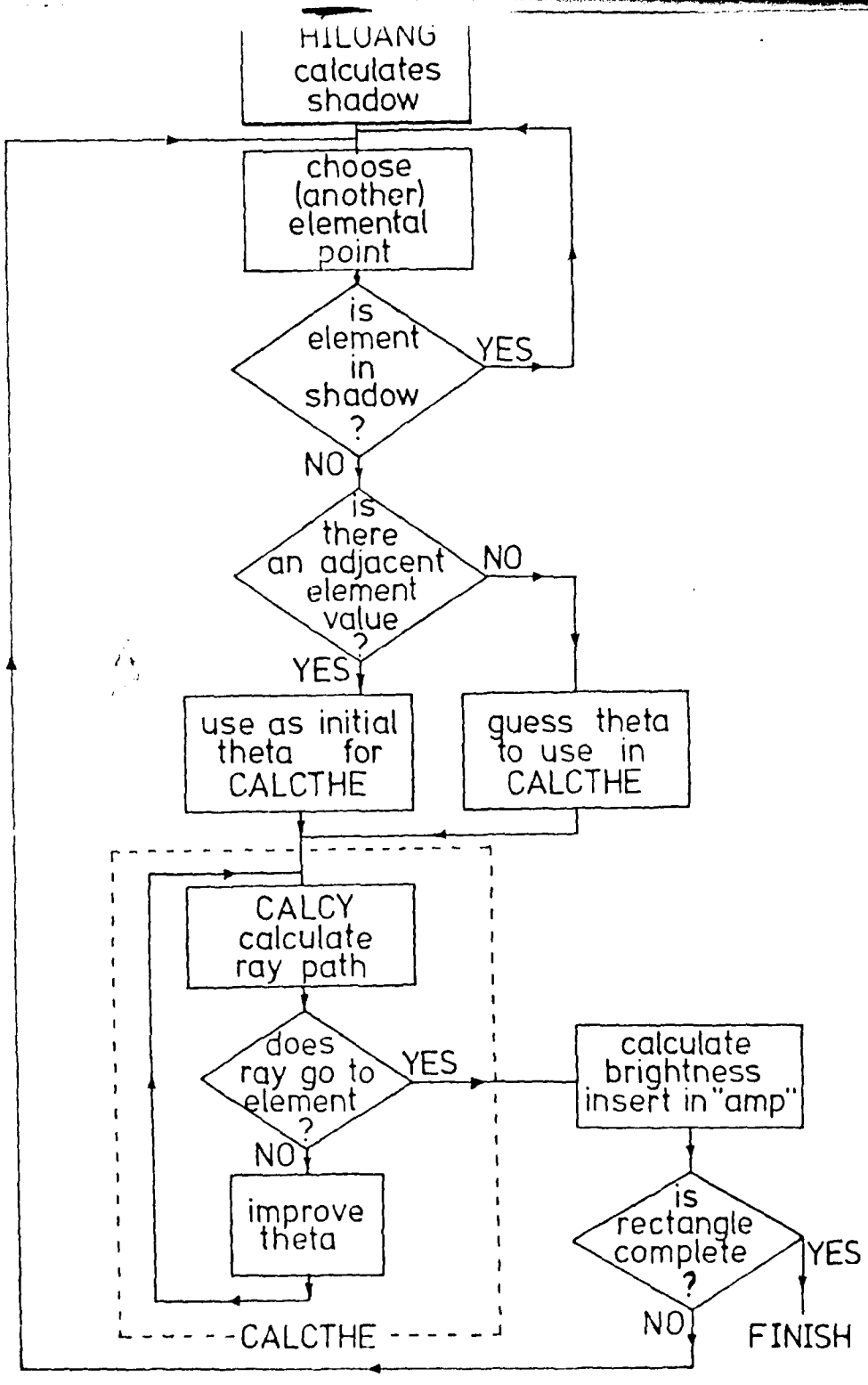

Figure 17. Flow diagram of program REFPATH.

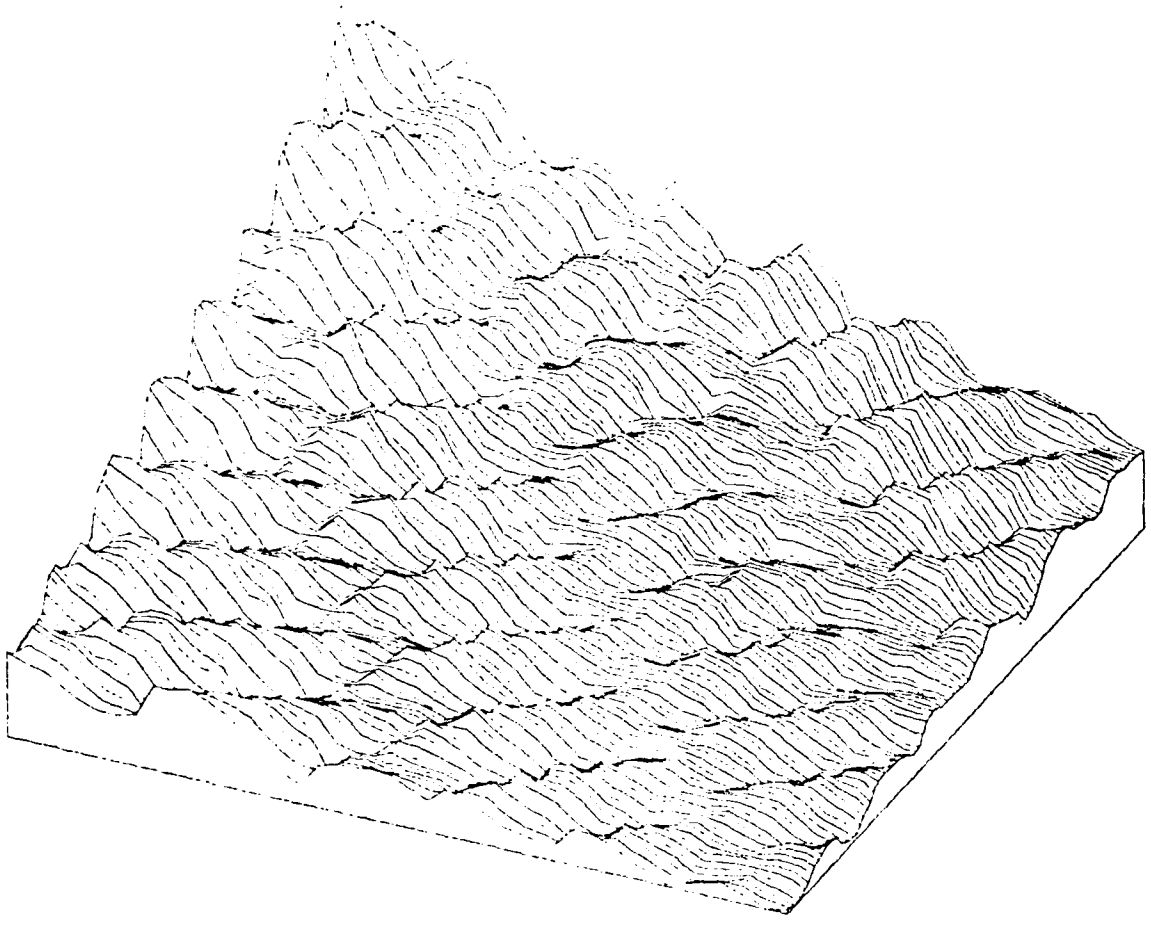

Figure 18. SYMVU representation for steel specimen with 1 mm radius hole.

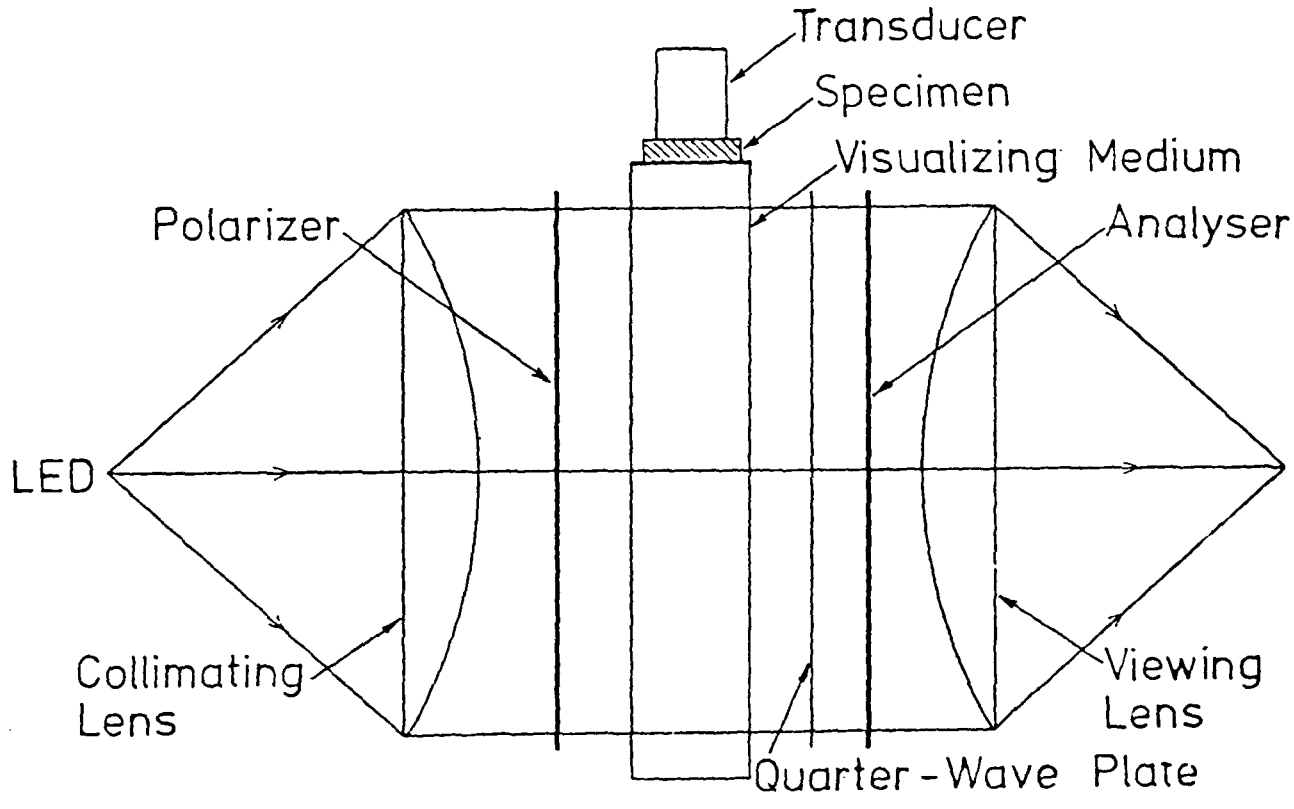

Figure 19. Schematic diagram of photoelastic system.

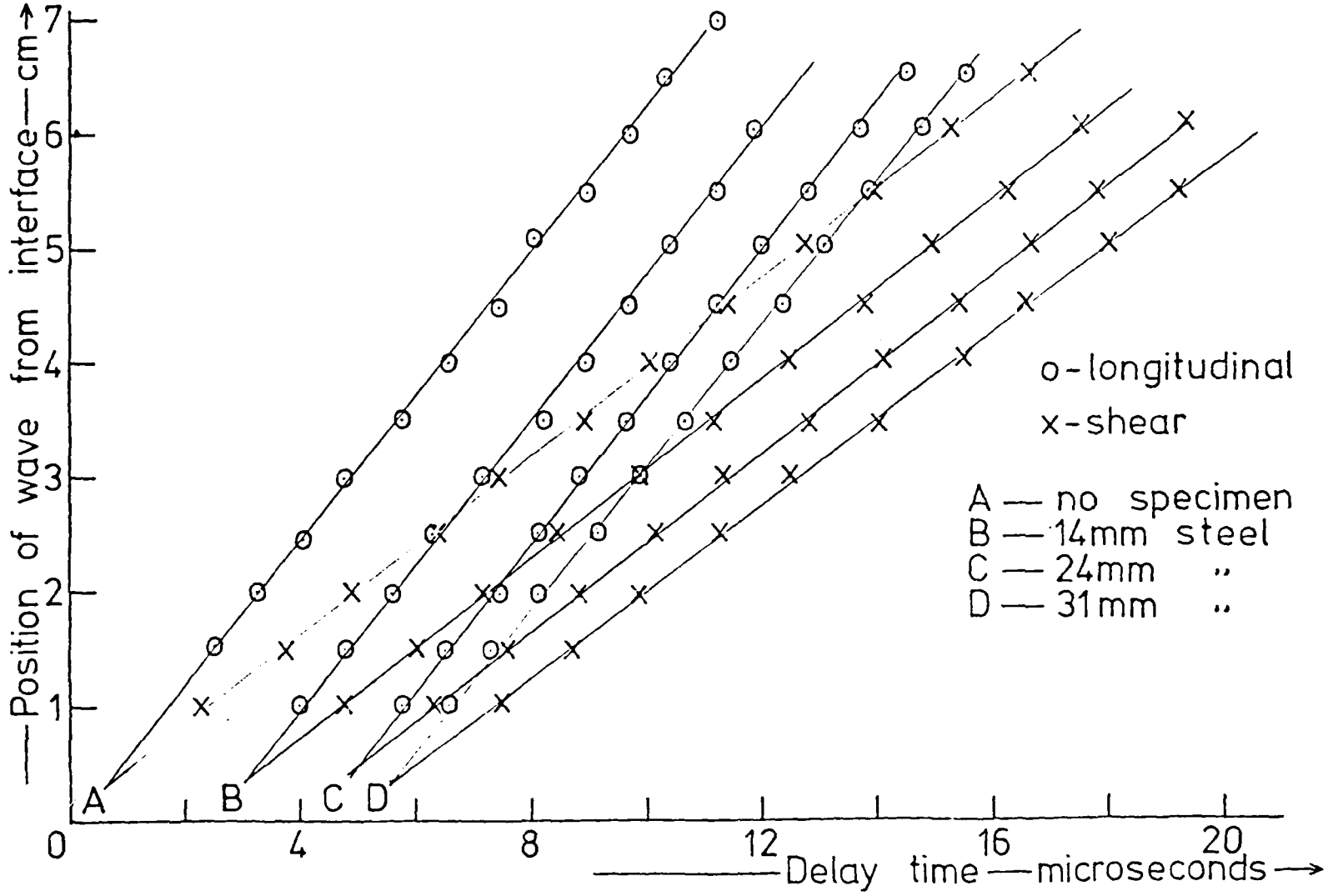

Figure 20. Position of longitudinal and shear wavefronts vs. delay.

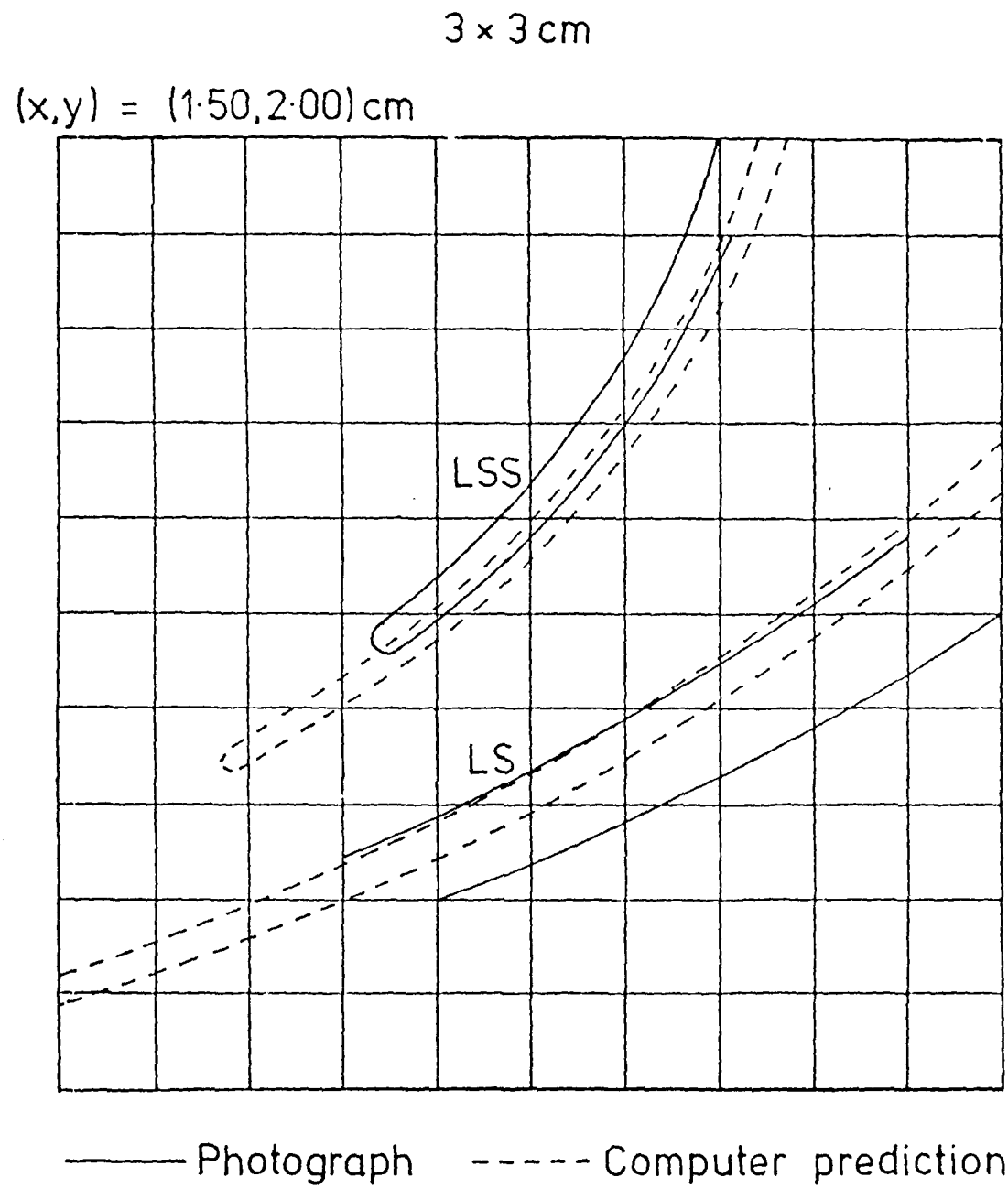

Figure 21. Computer simulation.

3 × 3 cm

(x,y) = (1·50, 2·00) cm

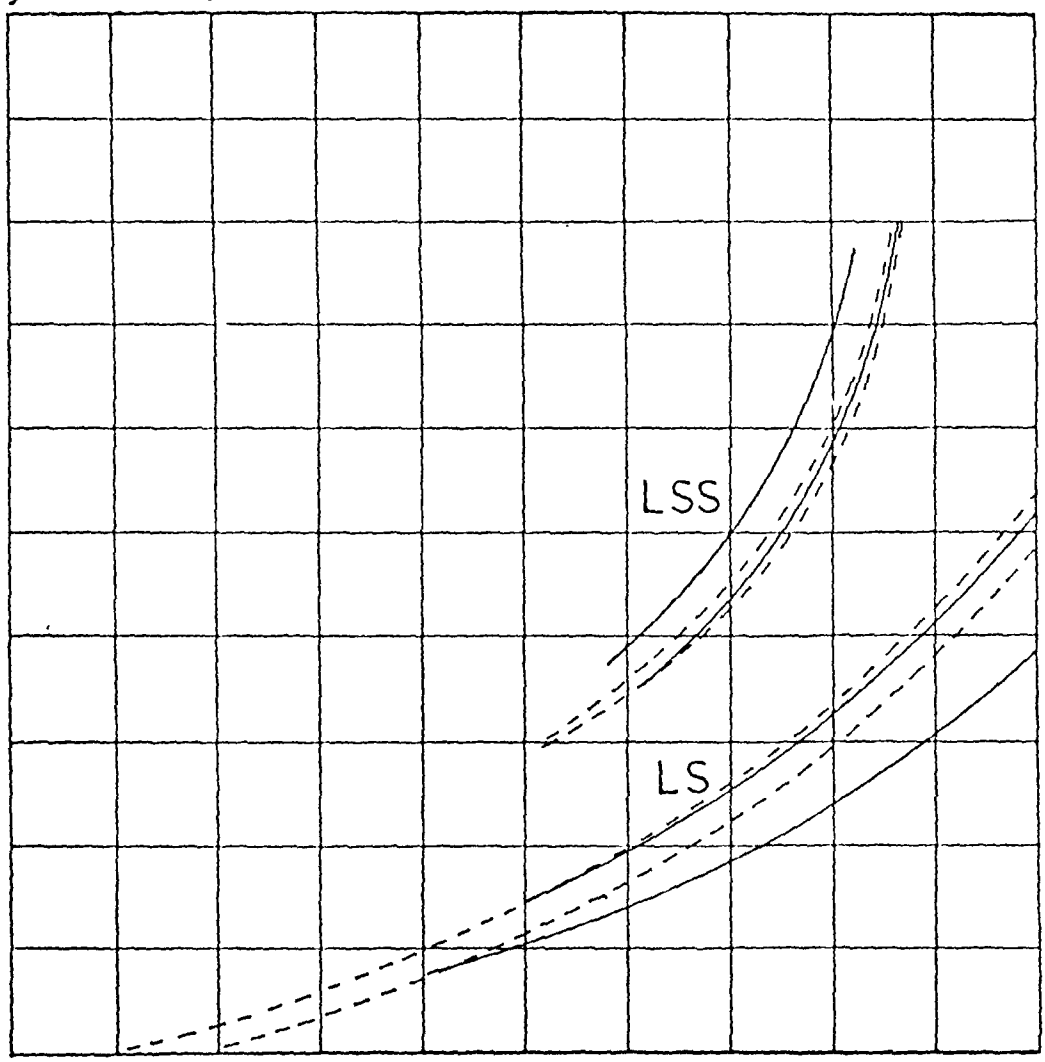

——— Photograph ----- Computer prediction

Photograph-Printout Comparison

Delay = 13·4 μs

Figure 22. Computer simulation.

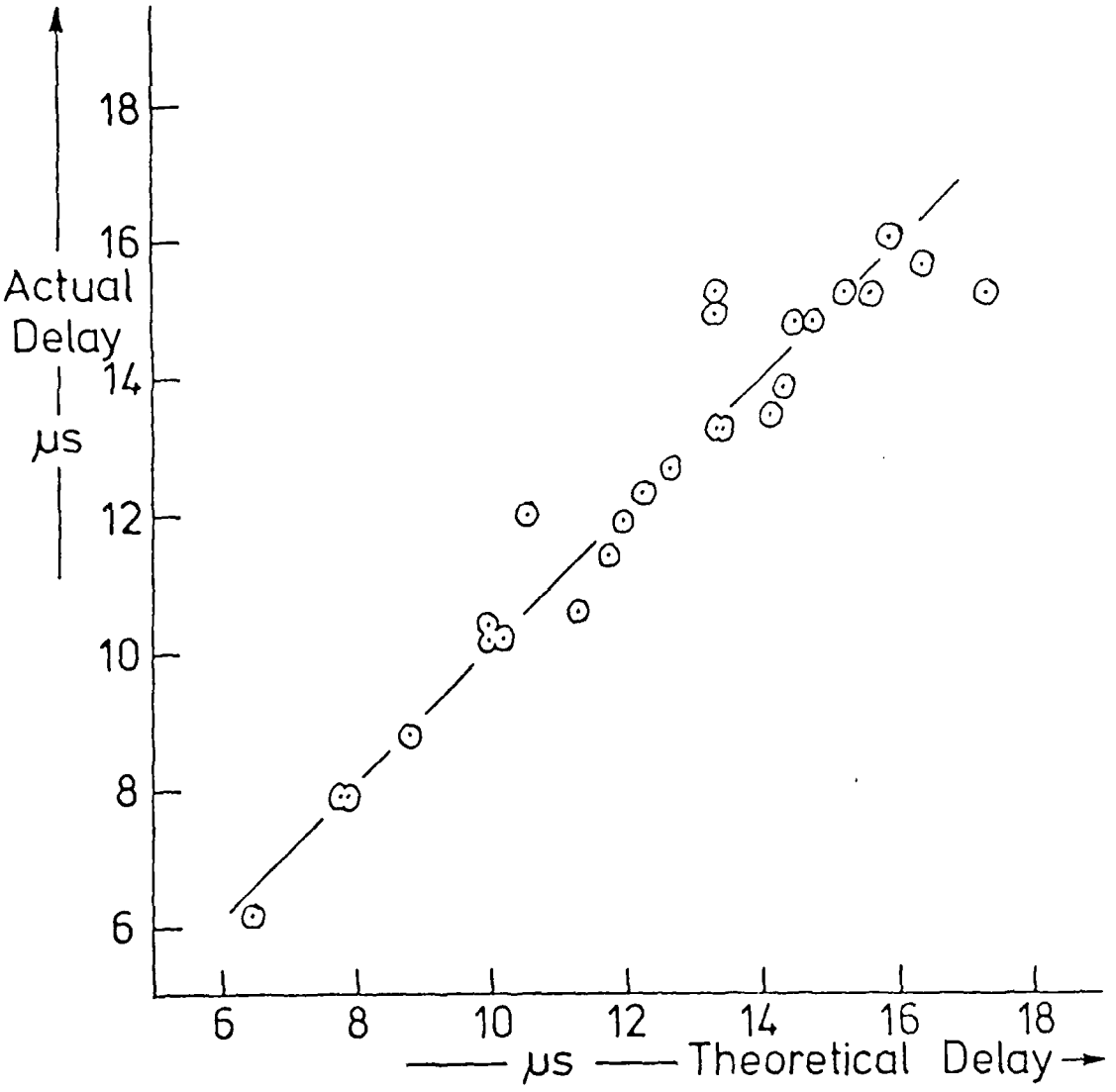

Figure 23. Experimental vs. theoretical delays.

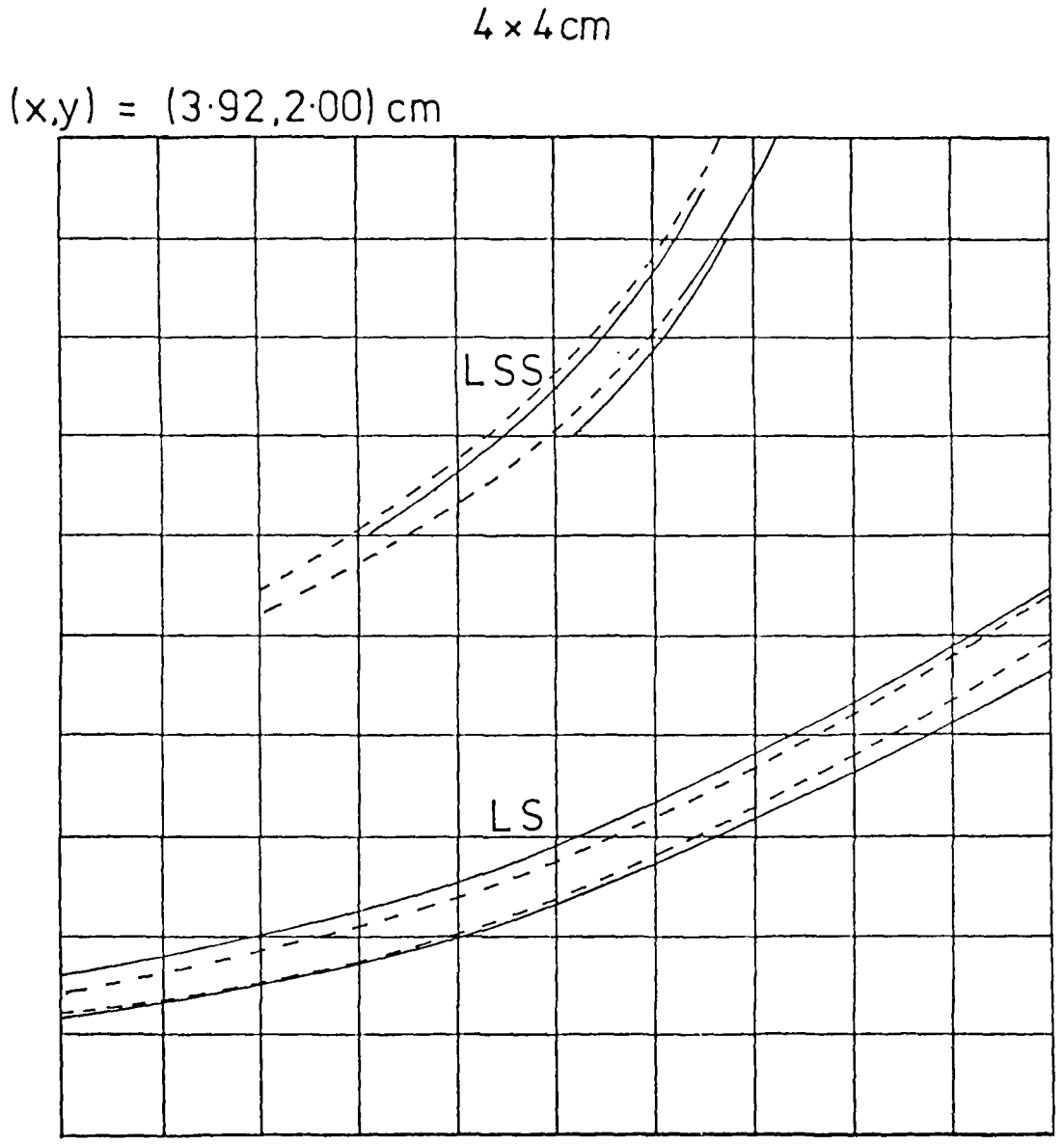

Figure 24. Computer simulation.

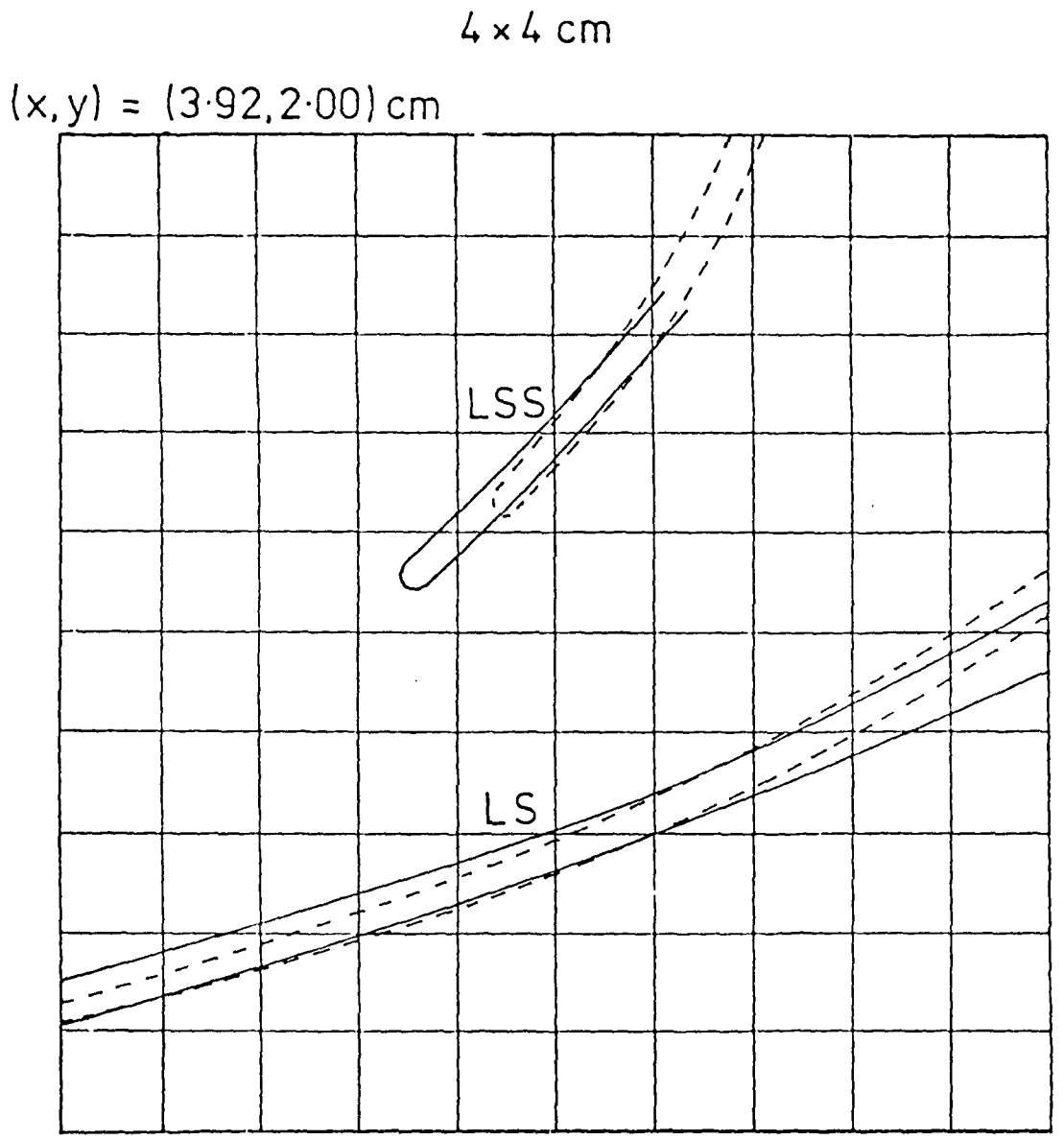

Figure 25. Computer simulation.

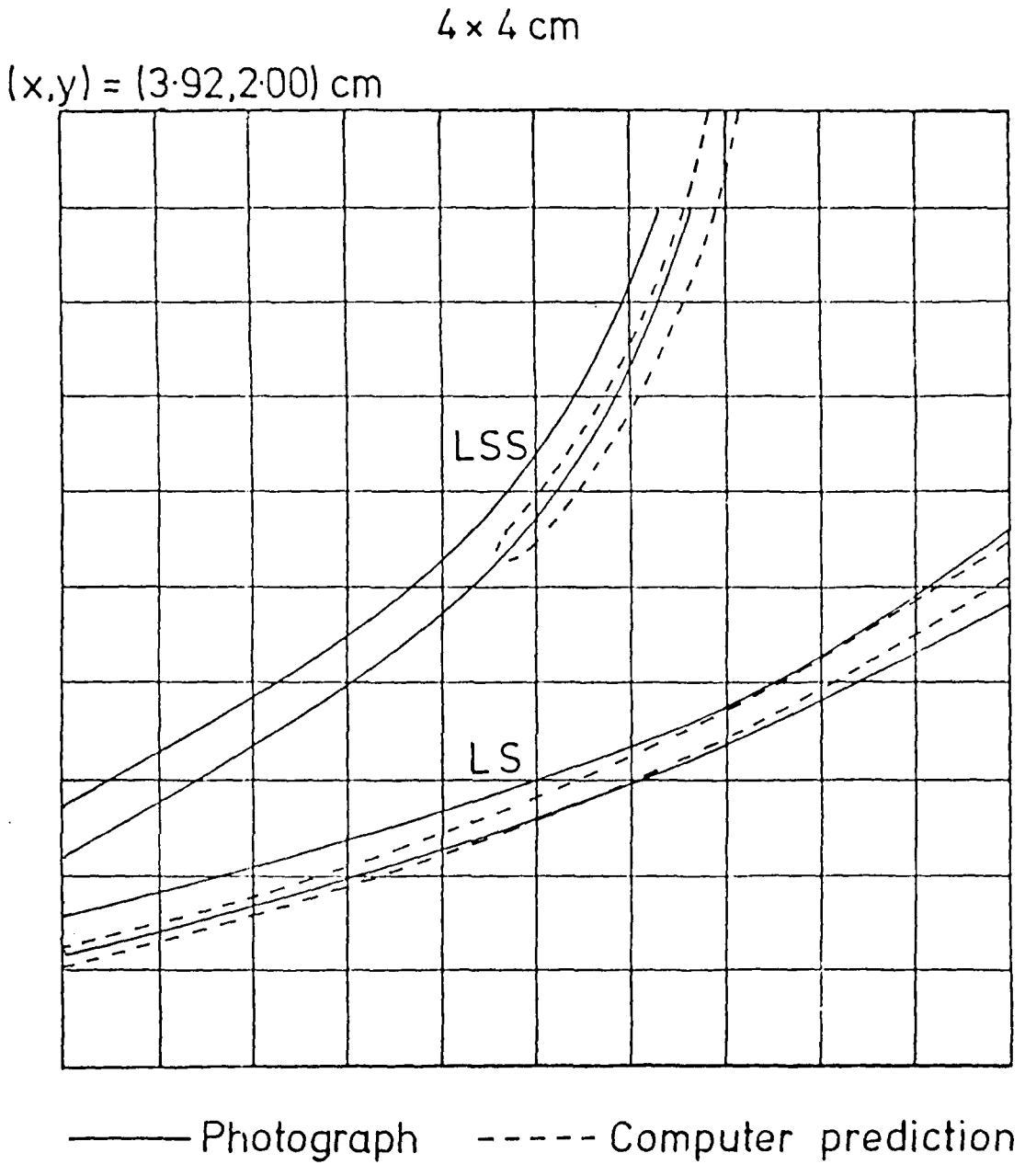

Figure 26. Computer simulation.

Figure 27. Interference pattern from reflected shear wave (LSS) from a 1 mm radius hole in steel (multiflash).

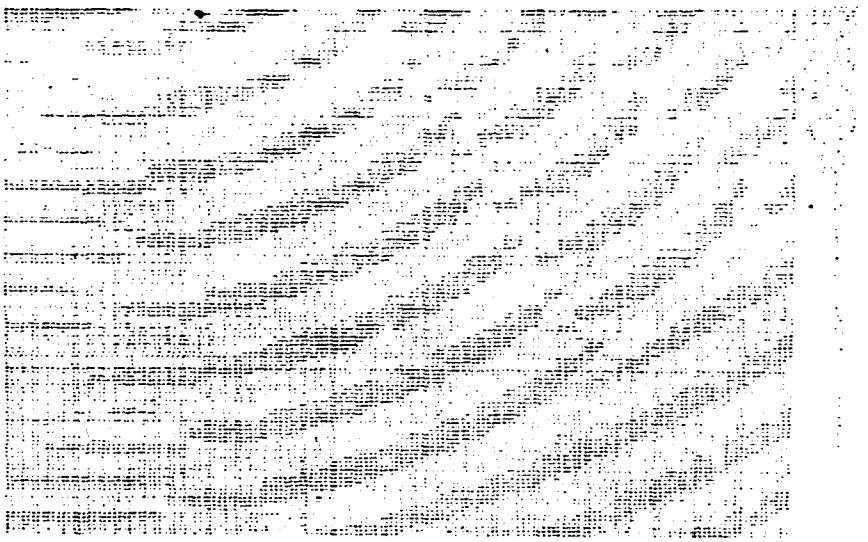

Figure 28. Computer simulation of Figure 27.